Plant Communications
Research Article

CellPress
Partner Journal

OPAQUE3, encoding a transmembrane bZIP transcription factor, regulates endosperm storage protein and starch biosynthesis in rice

Ruijie Cao[1,3], Shaolu Zhao[1,2,3], Guiai Jiao[1], Yingqing Duan[1], Liuyang Ma[1], Nannan Dong[1], Feifei Lu[1], Mingdong Zhu[1], Gaoneng Shao[1], Shikai Hu[1], Zhonghua Sheng[1], Jian Zhang[1], Shaoqing Tang[1], Xiangjin Wei[1,*] and Peisong Hu[1,*]

[1]State Key Laboratory of Rice Biology, China National Center for Rice Improvement, China National Rice Research Institute, Hangzhou 310006, China

[2]Institute of Agricultural Science in Jiangsu Coastal Areas, Yancheng 224002, China

[3]These authors contributed equally to this article.

***Correspondence: Xiangjin Wei (weixiangjin@caas.cn), Peisong Hu (hupeisong@caas.cn, hupeisong@caas.cn)**

https://doi.org/10.1016/j.xplc.2022.100463

ABSTRACT

Starch and storage proteins are the main components of rice (*Oryza sativa* L.) grains. Despite their importance, the molecular regulatory mechanisms of storage protein and starch biosynthesis remain largely elusive. Here, we identified a rice opaque endosperm mutant, *opaque3* (*o3*), that overaccumulates 57-kDa proglutelins and has significantly lower protein and starch contents than the wild type. The *o3* mutant also has abnormal protein body structures and compound starch grains in its endosperm cells. *OPAQUE3* (*O3*) encodes a transmembrane basic leucine zipper (bZIP) transcription factor (OsbZIP60) and is localized in the endoplasmic reticulum (ER) and the nucleus, but it is localized mostly in the nucleus under ER stress. We demonstrated that O3 could activate the expression of several starch synthesis-related genes (*GBSSI*, *AGPL2*, *SBEI*, and *ISA2*) and storage protein synthesis-related genes (*OsGluA2*, *Prol14*, and *Glb1*). O3 also plays an important role in protein processing and export in the ER by directly binding to the promoters and activating the expression of *OsBIP1* and *PDIL1-1*, two major chaperones that assist with folding of immature secretory proteins in the ER of rice endosperm cells. High-temperature conditions aggravate ER stress and result in more abnormal grain development in *o3* mutants. We also revealed that OsbZIP50 can assist O3 in response to ER stress, especially under high-temperature conditions. We thus demonstrate that O3 plays a central role in rice grain development by participating simultaneously in the regulation of storage protein and starch biosynthesis and the maintenance of ER homeostasis in endosperm cells.

Key words: grain development, ER stress, OPAQUE3, high temperature, rice

Cao R., Zhao S., Jiao G., Duan Y., Ma L., Dong N., Lu F., Zhu M., Shao G., Hu S., Sheng Z., Zhang J., Tang S., Wei X., and Hu P. (2022). *OPAQUE3*, encoding a transmembrane bZIP transcription factor, regulates endosperm storage protein and starch biosynthesis in rice. Plant Comm. **3**, 100463.

INTRODUCTION

Rice is a staple food for more than half of the world's population. Starch and storage proteins determine the yield and quality of rice grains; they account for approximately 80% and 10% of rice grain weight, respectively. Starch is composed of linear amylose and multi-branched, semi-crystalline amylopectin. Its biosynthesis in plant endosperm involves a series of key enzymes that function coordinately. ADP-glucose pyrophosphorylase is responsible for the synthesis of ADP-glucose, which is the major substrate for starch synthesis (Beckles et al., 2001; Nakamura, 2002). Amylose is synthesized by granule-bound starch synthase I (GBSSI) through progressive addition of ADP-glucose to linear chains of α(1-4)-linked glucose residues. Amylopectin synthesis requires synergistic cooperation of soluble starch synthases, branching enzymes, and debranching enzymes (Ball and Morell, 2003). Many natural variations or artificial mutations of these genes cause abnormal endosperm phenotypes or grain-filling defects (Nishi et al., 2001; Umemoto et al., 2004; Tian et al., 2009; Wei et al., 2017; Zhang et al., 2019a). Rice grain storage proteins also determine rice quality and are classified

Published by the Plant Communications Shanghai Editorial Office in association with Cell Press, an imprint of Elsevier Inc., on behalf of CSPB and CEMPS, CAS.

This is an open access article under the CC BY-NC-ND license (http://creativecommons.org/licenses/by-nc-nd/4.0/).

into glutelin, globulin, prolamin, and albumin according to their solubility. Prolamins are synthesized and processed in the endoplasmic reticulum (ER) lumen, and they then aggregate and bud off to form the spherical protein body I (PBI) (Li et al., 1993). The 57-kDa proglutelins are synthesized in the ER and later trafficked to protein storage vacuoles (PSVs) through dense vesicles (DVs) to be processed into mature acidic and basic subunits, eventually forming the irregularly shaped protein body II (PBII) together with α-globulin (Yamagata et al., 1982; Washida et al., 2012). The genes that participate in processing and trafficking of storage proteins have been well investigated, including *GPA1–GPA8*. Loss of function of these genes often results in floury grains with abnormal protein bodies (Wang et al., 2010, 2016; Liu et al., 2013; Ren et al., 2014, 2020; Zhu et al., 2019, 2021; Pan et al., 2021).

Some transcription factors (TFs) have been reported to play important roles in regulation of rice endosperm starch and storage protein biosynthesis. Rice starch regulator 1 (RSR1) negatively regulates expression of type I starch synthesis genes. The knockout mutant *rsr1* has a larger grain size with increased amylose content and altered fine structure of amylopectin and starch morphology compared with the wild type (Fu and Xue, 2010). NF-YB1 can directly bind to the "CCAAT boxes" of Os*SUT1*, Os*SUT3* and Os*SUT4* to activate their expression, regulating sucrose loading to the developing endosperm for starch biosynthesis (Bai et al., 2016). NF-YB1 can also interact with NF-YC12, bHLH144, or OsERF115 to form a transcription complex that directly binds to the "G box" or "GCC box" in promoters of genes involved in starch synthesis and sugar and amino acid transport (Xu et al., 2016; Bello et al., 2019; Xiong et al., 2019). OsbZIP58 regulates starch synthesis and aleurone layer number by directly binding to the promoters of starch synthesis-related genes (*OsAGPL3*, *Wx*, *OsSSIIa*, *SBE1*, *OsBEIIb*, and *ISA2*) and activating their expression (Wang et al., 2013). OsbZIP58 can also interact with rice prolamin box binding factor (RPBF) and activate expression of the rice grain storage protein synthesis-related genes *GluA1*, *GluA2*, *GluA3*, *GluB1*, *GluD1*, *10-kDa prolamin*, *13-kDa prolamin*, and *16-kDa prolamin* (Kawakatsu et al., 2009). In maize, ZmNAC128 and ZmNAC130 can bind to the "ACGCAA" motif to activate transcription of the *Bt2* and *16-kDa γ-zein* genes, thus having a pleiotropic effect on biosynthesis of grain storage protein and starch (Zhang et al., 2019b). A similar mechanism has been reported for rice OsNAC20 and OsNAC26; simultaneous knockout of these two TFs significantly decreases starch and protein accumulation and grain weight and alters starch granule formation (Wang et al., 2020).

The ER is the major organelle for storage protein synthesis, folding, and export (Sun et al., 2021). Overaccumulation of unfolded proteins in the ER causes ER stress and activates the unfolded protein response (UPR), which subsequently increases expression of ER chaperone genes to maintain ER homeostasis (Howell, 2013). The UPR signaling pathway has been well elucidated in *Arabidopsis*; the bZIP TF AtbZIP60 is normally localized in the ER lumen through the transmembrane domain (TMD) in its C-terminal region. When stress is sensed in the ER, the TMD is cleaved by the ribonuclease AtIRE1, and the cytoplasmic N-terminal activation domain is transferred to the nucleus to upregulate ER stress-related chaperone genes (Iwata and Koizumi, 2005; Deng et al., 2011). Otherwise, AtbZIP17 and AtbZIP28 are cleaved by Golgi apparatus-localized S2P proteases under ER stress, and their cytoplasmic portion, including a bZIP domain, is then released to the nucleus to activate UPR genes for maintenance of ER homeostasis (Liu et al., 2007; Iwata et al., 2017). In rice, OsbZIP39 and OsbZIP50, the orthologs of *Arabidopsis* AtbZIP17 and AtbZIP60, are also cleaved and transferred to the nucleus from the ER to upregulate chaperone genes under ER stress (Hayashi et al., 2012; Takahashi et al., 2012). Binding proteins (BiPs) are ER chaperones that can interact with nascent immature secretory proteins and assist with protein folding in concert with other chaperones such as protein disulfide isomerase-like (PDIL) proteins in the ER lumen (Bertolotti et al., 2000; Pobre et al., 2019). Severe suppression or extreme overexpression of *OsBiP1* can result in floury endosperm with abnormal protein bodies and reductions in grain weight, endosperm storage protein content, and starch accumulation (Yasuda et al., 2009; Wakasa et al., 2011). PDIL1-1 participates in the maturation of proglutelin in the ER in rice endosperm, and absence of PDIL1-1 also leads to the UPR and the formation of floury endosperm (Satoh-Cruz et al., 2010; Han et al., 2012). High temperature during the rice grain-filling stage can induce more serious ER stress, resulting in a higher grain chalkiness rate with a lower yield (Howell, 2013; Ren et al., 2021). Although bZIP TFs are known to play important roles in response to ER stress, the molecular mechanisms by which bZIP TFs respond to high temperature and regulate grain starch and storage protein biosynthesis in rice remain unclear.

Here, we identified a rice opaque endosperm mutant, *opaque 3* (*o3*). *OPAQUE3* (*O3*) encodes a transmembrane bZIP TF (OsbZIP60) that can directly bind to and activate the ER chaperone genes *OsBiP1* and *PDIL1-1* and endosperm storage protein and starch biosynthesis-related genes. It thus regulates ER homeostasis and affects grain starch and storage protein biosynthesis, especially under high-temperature conditions. These findings enhance our understanding of the genetic basis of ER stress responses and grain filling in rice, providing useful information for genetic improvement of grain yield and quality.

RESULTS

The *o3* mutant accumulates 57-kDa proglutelins and displays defects in grain filling

To understand the molecular mechanisms of grain filling and quality formation, we identified a rice mutant, *o3*, with opaque and floury endosperm from a rice mutant library induced by ethyl methanesulfonate (EMS) treatment of *japonica* 'Zhonghua11' (Figure 1A and 1B). The *o3* mutant had a slower grain-filling rate than the wild type; the weight of developing grain from 12 days after fertilization (DAF) and the grain setting rate, 1000-grain weight, and grain yield per plant were significantly lower in the *o3* mutant compared with the wild type (Figure 1C–1G). Except for significantly reduced grain thickness, there were no visible differences in plant morphology and grain shape between the *o3* mutant and the wild type (Supplemental Figure 1). Next, we measured the contents of storage substances in mature endosperm of the wild type and the *o3* mutant. The total starch, amylose, and total protein contents were significantly lower in *o3* endosperm compared with wild-type endosperm, whereas the total lipid content was higher (Figure 1H–1K). Storage

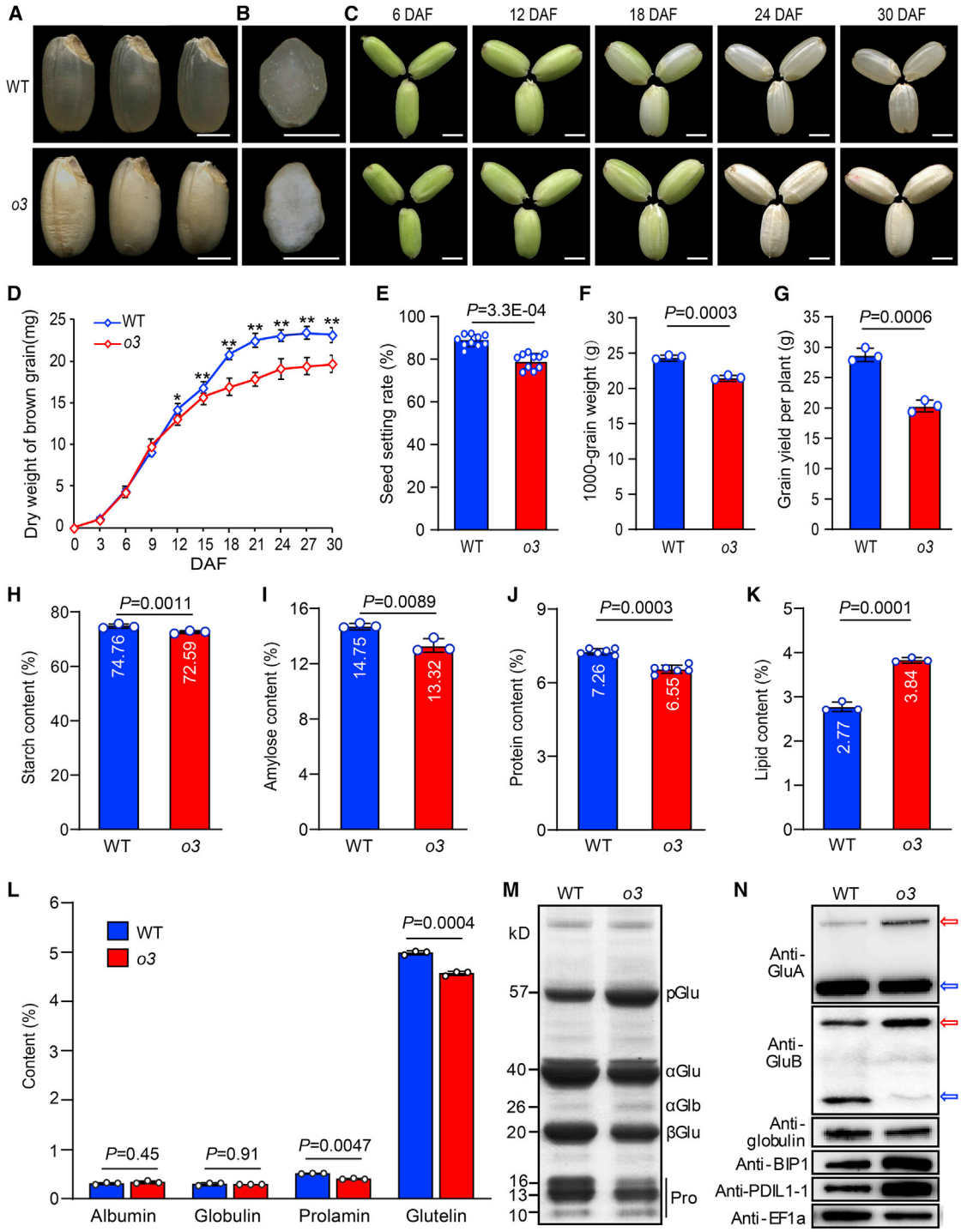

Figure 1. Characterization of the *opaque3* (*o3*) mutant.

(A) Appearance of wild-type (WT) and *o3* mutant brown rice.

(B) Transverse sections of WT and *o3* endosperm.

(C) Fresh WT and *o3* grains at various stages of development. DAF, days after fertilization. Scale bars, 2 mm in **(A–C)**.

(D) Dry weight of WT and *o3* grains at various stages of grain filling.

(E–G) WT and *o3* seed setting rate **(E)**, 1000-grain weight **(F)**, and grain yield per plant **(G)**.

(H–K) The percent content of total starch **(H)**, amylose **(I)**, total protein **(J)**, and lipid **(K)** in WT and *o3* endosperm.

(L) Storage protein content in WT and *o3* milled rice.

(M) SDS-PAGE profiles of total storage proteins in WT and *o3* dry grain. pGlu, 57-kDa proglutelin; αGlu, 40-kDa glutelin acidic subunit; αGlb, 26-kDa α-globulin; βGlu, 20-kDa glutelin basic subunit; Pro, prolamin.

(legend continued on next page)

protein contents, including those of glutelin and prolamin, were also significantly lower in *o3* endosperm (Figure 1L). An SDS-PAGE assay of total protein showed that 57-kDa proglutelins were overaccumulated, whereas the amounts of 20-kDa basic and 40-kDa acidic subunits of mature glutelins were reduced. Prolamins were also notably decreased in endosperm of *o3* compared with the wild type (Figure 1M). The higher amount of 57-kDa proglutelins in *o3* endosperm was confirmed by immunoblotting with isoform-specific antibodies (GluA and GluB). The protein levels of two key molecular chaperones, BIP1 and PDIL1-1, were greatly elevated in the *o3* mutant (Figure 1N). These chaperones are known to be induced in 57H rice mutants defective in maturation and export of proglutelins from the ER (Takemoto et al., 2002; Wang et al., 2016). These results indicate that *o3* is a 57-kDa proglutelin overaccumulation mutant and may be defective in the maturation and exit of proglutelins from the ER.

O3 is involved in storage protein processing and export from the ER in developing endosperm cells

We prepared semi-thin sections (0.5 μm) of 12-DAF endosperm from *o3* mutant and wild-type plants and subjected them to Coomassie blue staining to explore the cellular basis of abnormal accumulation of the glutelin precursor in the *o3* mutant. Two types of protein bodies, irregularly shaped PBIIs and round PBIs, were observed in *o3* and wild-type endosperm, and there were no significant differences in the numbers of PBI and PBII between *o3* and the wild type (Supplemental Figure 2A and 2B). Transmission electron microscopy assays were performed to observe the structure of protein bodies in the 12-DAF endosperm. In *o3* endosperm cells, the ER morphology was more bent and irregular, some small protein bodies remained in the ER terminal, and many ER-derived vesicles with or without protein bodies were observed (Figure 2A–2F). Unusual fusion of PBII and PBI as well as fragmented protein bodies were observed in the developing endosperm of *o3* (Figure 2H and 2I and Supplemental Figure 2C and 2D). Otherwise, there were no obvious differences in the morphology or structure of the Golgi apparatus or DVs between *o3* and wild-type endosperm (Figure 2B, 2C, and 2G). These results suggest that *O3* plays an important role in processing and export of storage proteins from the ER in rice endosperm cells.

O3 regulates formation of compound starch grains in endosperm cells

We next observed the morphology of starch grains in endosperm cells of *o3* and the wild type. Scanning electron microscopy (SEM) of transverse sections from mature endosperm showed that wild-type endosperm cells were filled with densely packed and irregular polyhedral starch granules (SGs), whereas *o3* endosperm cells contained spherical and loosely packed SGs (Supplemental Figure 2E and 2F). Semi-thin sections of developing endosperm at 9 DAF were prepared to observe the formation of compound starch grains in *o3* and the wild type. Fewer well-developed compound grains and some immature compound grains were observed in peripheral endosperm cells of the wild type and *o3* mutant (Figure 2J and 2M). In the center of wild-type endosperm, most amyloplasts produced compound grains consisting of several dozen SGs (Figure 2K and 2L). However, fewer compound grains and more single and dispersed SGs were observed in central cells of *o3* endosperm (Figure 2N and 2O and Supplemental Figure 2S and 2T). We then used transmission electron microscopy to observe the development of compound starch grains. Wild-type amyloplasts were filled with polyhedral SGs, which quickly occupied the interior space during grain development, eventually forming a typical complex structure (Supplemental Figure 2G–2I). Similar to the wild type, there were few well-developed amyloplasts in endosperm cells of the *o3* mutant (Supplemental Figure 2J–2L). However, the *o3* mutant had many disintegrated amyloplasts during the early developmental stage, and the SGs were dispersed throughout the central endosperm cells (Supplemental Figure 2M–2O). There were abundant round and small single SGs instead of compound grains in developing endosperm cells of the *o3* mutant (Supplemental Figure 2P–2R), consistent with the results observed in the semi-thin sections (Figures 2N–2O). These results suggest that *O3* regulates the formation of starch compound grains in endosperm cells during rice grain development.

We also examined more starch physicochemical properties and the fine structure of wild-type and *o3* endosperm. First, the chain length distribution of amylopectin was tested, and the results showed that the proportion of short chains with degree of polymerization values between 6 and 12 was higher in the *o3* mutant compared with the wild type, whereas the proportion of intermediate chains with degree of polymerization values in the range of 14–26 was lower (Supplemental Figure 3A). The viscosity of *o3* starch was lower and the gelatinization enthalpy (ΔH) of *o3* starch was significantly higher than that of wild-type starch (Supplemental Figure 3B and 3C). The *o3* endosperm starch was slightly harder to gelatinize in 4–6 mol/L urea compared with wild-type starch (Supplemental Figure 3D). These results show that the physicochemical properties of endosperm starch were altered in the *o3* mutant.

O3 encodes a transmembrane bZIP TF

We used a marker mapping and MutMap combination method to clone the gene responsible for the *o3* mutation phenotype. First, we selected 207 individuals showing the *o3* phenotype from the F_2 population derived from a cross between *o3* and Nanjing11 (*indica*). The mutation locus was first mapped to the long arm of chromosome 7 between the markers RM22097 and RM22166 (Figure 3A). Next, we selected 40 individuals with opaque grains from the F_2 population of a cross between *o3* and the wild type and then sequenced pooled DNA from the selected individuals and wild-type plants

(N) Immunoblot analysis of GluA, GluB, globulin, and the molecular chaperones BiP1 and PDIL1-1. Red arrows denote 57-kDa proglutelins. Blue arrows denote the glutelin acidic subunits. EF1α was used as a loading control.

Data in **(D–L)** are means ± SD from at least three biological replicates. Statistically significant differences were determined using Student's *t*-test (*$P < 0.05$, **$P < 0.01$). *P* values are shown in **(E–L)** when statistically significant.

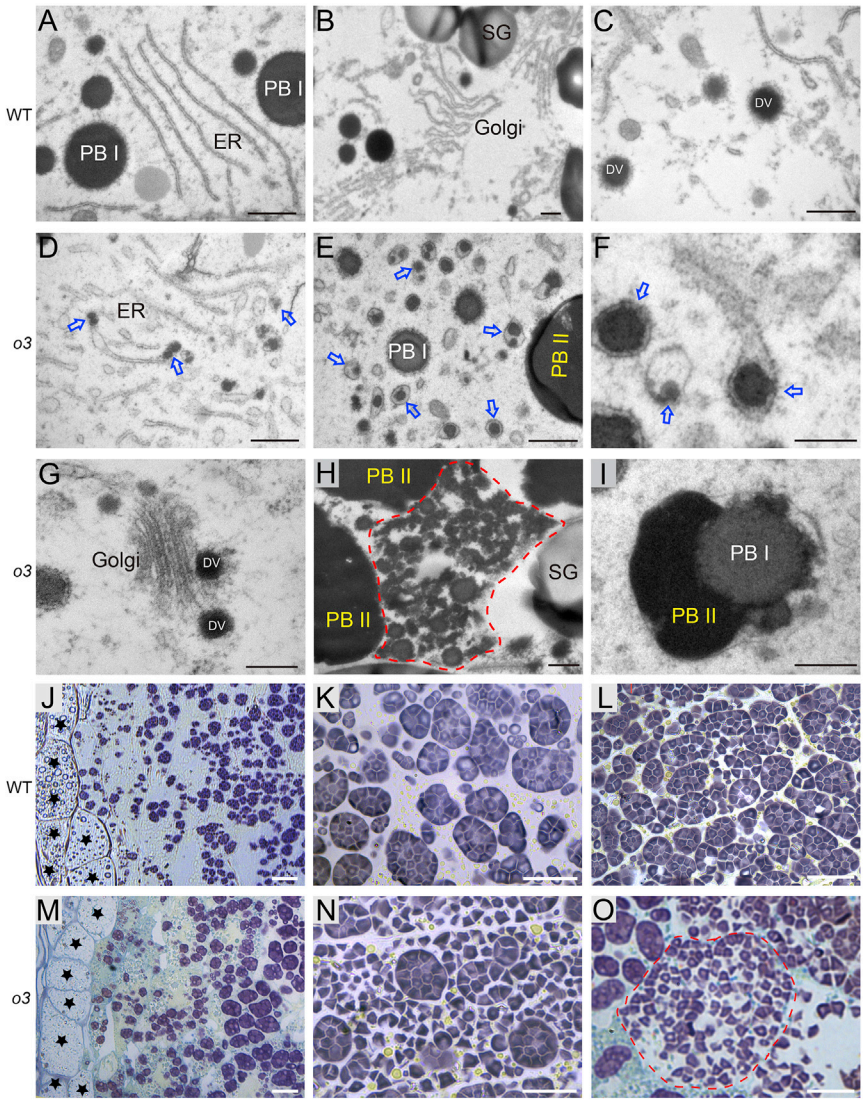

Figure 2. Protein body and starch grain development in WT and *o3* mutant endosperm cells.

(A) Endoplasmic reticulum (ER) and protein body I (PBI) were observed in WT endosperm cells at 12 DAF.

(B and C) The Golgi apparatus and dense vesicles (DVs) in WT endosperm cells.

(D–F) Small protein bodies (blue arrows) remaining in the terminal of ER or ER-derived vesicles and PBI or PBII were observed in *o3* endosperm cells.

(G) The Golgi apparatus and DVs in *o3* endosperm cells.

(H) The structure of fragmentized protein bodies (red dotted box) was observed in *o3* endosperm cells.

(I) The structure of the fusion of PBI and PBII was observed in *o3* endosperm cells.

(J–O) Semi-thin sections of WT **(J–L)** and *o3* **(M–O)** endosperm at 9 DAF.

(J and M) The peripheral region of the endosperm.

(K, L, N, and O) The central region of the endosperm.

Stars indicate aleurone cells in **(J)** and **(M)**. Red dotted lines indicate an endosperm cell of *o3* filled with abundant single and dispersed starch granules (SGs). Scale bars, 1 μm **(A–E)**, **(H)**, and **(I)**, 0.2 μm **(F)** and **(G)**, and 20 μm **(J–O)**.

using the Illumina HiSeq PE150 platform. Using the MutMap approach described by Abe et al. (2012), we detected a single peak in the primary mapping region on chromosome 7 that contained 13 SNPs with a SNP index greater than 0.8 (Figure 3B and Supplemental Figure 4). Among these SNPs, a nonsynonymous SNP (C to T) in the first exon of LOC_Os07g44950 in the *o3* mutant caused leucine[139] to be replaced by proline[139] in the encoded protein (Figure 3C).

To verify whether *LOC_Os07g44950* was the gene responsible for the mutant phenotype, we transformed the *o3* mutant with a complementation vector carrying the *O3* genomic sequence, including its native promoter. Grains harvested from independent T_1 complementation lines showed phenotypes similar to the wild type (Figure 3D). The 1000-grain weight and the contents of total starch, amylose, and total protein in endosperm of complementation lines were similar to those in the wild type (Figure 3E–3I). We also knocked out *LOC_Os07g44950* in the wild type using CRISPR-Cas9 editing and successfully obtained four independent homozygous mutants (Supplemental Figure 5A). These mutants exhibited opaque grains with reduced grain weight, and the contents of total starch, amylose, and total protein were similar to those of the *o3* mutant (Figure 3D–3I and Supplemental Figure 5B–5D). SGs in endosperm cells of complementation and knockout mutant lines also exhibited granule morphologies similar to those of the wild type and *o3* mutant, respectively (Figure 3D). SDS-PAGE showed that the level of storage protein subunits in complementation lines was restored to that in the wild type, and the level in knockout mutant lines was similar to that in the *o3* mutant (Figure 3J). Therefore, LOC_Os07g44950 (*O3*) is the gene responsible for the *o3* phenotype. We also performed *O3* overexpression (OE) in the wild type; however, the positive OE lines showed no significant differences in plant architecture, grain appearance and weight, and storage substance contents in the endosperm compared with the wild type (Supplemental Figure 6).

O3 (LOC_Os07g44950) encodes a protein with 568 amino acids that was predicted to be a bZIP TF, OsbZIP60 (Nijhawan et al., 2008). O3 contains a bZIP DNA-binding domain followed by a TMD in the middle (Supplemental Figure 7A). A traditional transactivation test using yeast two-hybrid assays revealed that O3 has strong transcriptional activation ability and that the N-terminal region containing 82 amino acids is the critical transactivation domain (Supplemental Figure 7A). Phylogenetic analysis revealed that O3 shared high homology with other bZIP TFs, such as OsbZIP39, OsbZIP50, AtbZIP17, and AtbZIP28, in rice or *Arabidopsis* (Supplemental Figure 7B and 7C).

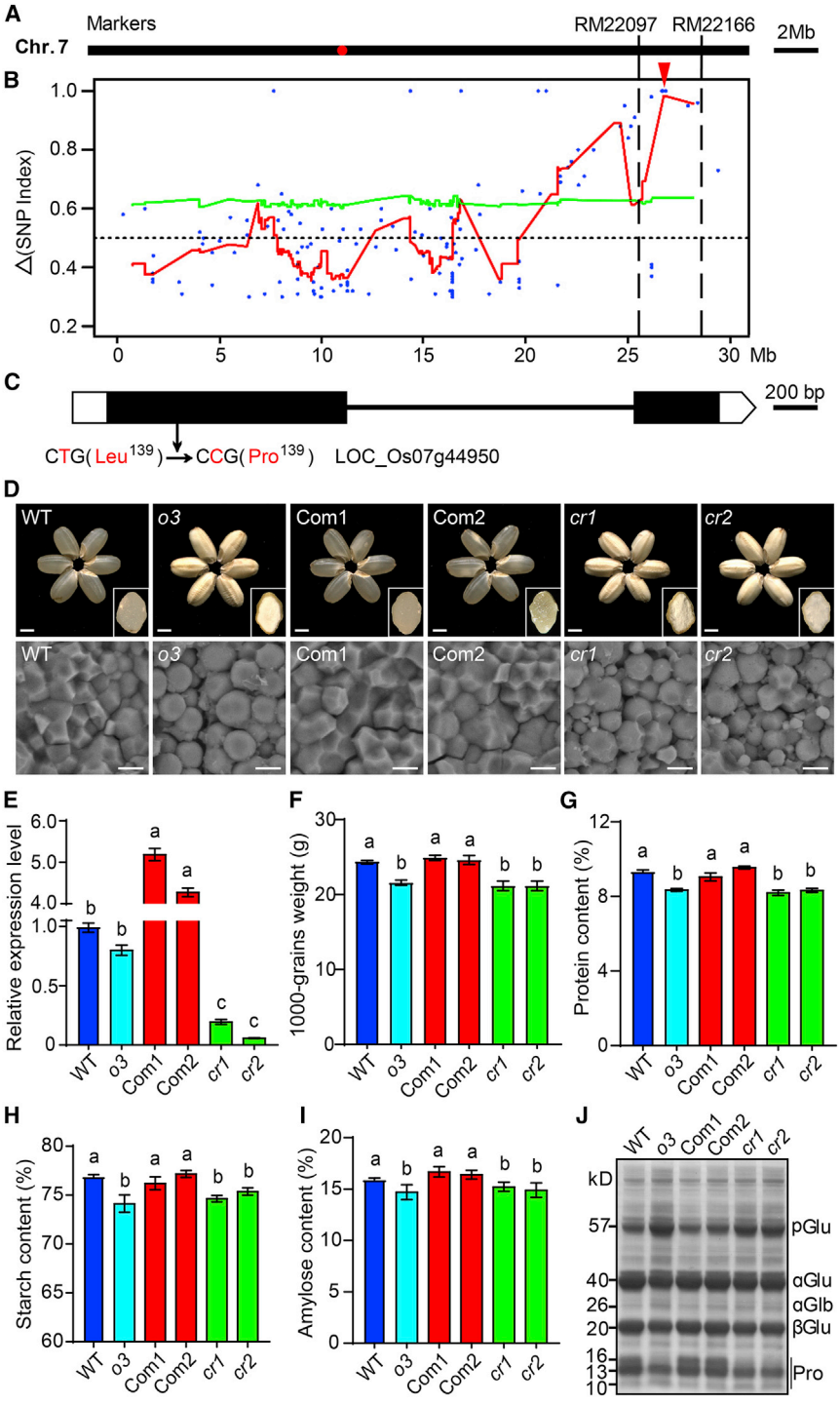

Figure 3. Identification of *Opaque3* (*O3*) using Map-based cloning and the MutMap method.

(A) The *O3* locus was first mapped to the long arm of chromosome 7 between the markers RM22097 and RM22166.

(B) Identification of genomic regions possibly harboring causal mutations for *o3* mutants using MutMap. The red curves represent SNP index plots on chromosome 7; the red arrowhead indicates a single peak detected in the primary mapping region.

(C) Gene structure and mutation site in *O3* (*LOC_Os07g44950*). A SNP (T to C) caused a change from Leu-139 to Pro-139 in the encoded protein.

(D) Grain appearance and SG morphology of the WT, *o3* mutant, complementation lines (*o3* mutant expressing *O3*; Com1 and Com2), and *O3* knockout lines (*cr1* and *cr2*). Insets show transverse sections of representative grains. Scale bars, 2 mm (top) and 5 μm (bottom).

(E) Relative expression level of *O3* in developing endosperm of WT, *o3*, Com1, Com2, *cr1*, and *cr2*.

(F–I) 1000-grain weight **(F)**, total protein content **(G)**, total starch content **(H)**, and amylose content **(I)** of WT, *o3*, Com1, Com2, *cr1*, and *cr2* grains. Data in **(E–I)** are means ± SD from at least three biological replicates. Significant differences are indicated by different letters according to Student's *t*-test.

(J) SDS-PAGE profiles of total storage proteins of WT, *o3*, Com1, Com2, *cr1*, and *cr2* dry grains.

O3 is highly expressed in grains, and the encoded bZIP TF is transferred to the nucleus under ER stress

We investigated the temporal and spatial expression patterns of *O3* using quantitative reverse transcriptase PCR (qRT–PCR). *O3* was constitutively expressed in all examined tissues, with higher levels in developing grains, young panicles, and leaves (Figure 4A). We then ectopically expressed the reporter gene *GUS* driven by the *O3* promoter in rice and examined GUS activity using histochemical analysis. GUS activity was more prominent in developing grains and young panicles, consistent with the qRT–PCR results (Figure 4B).

We next examined the subcellular localization of O3 by transiently expressing an O3-GFP fusion construct (*35S::O3:GFP*) in rice protoplasts and tobacco leaves. The GFP control protein was evenly distributed in the cytoplasm and nucleus. However, the O3-GFP fusion protein was present only in the nucleus and ER, based on co-localization with the DAPI signal of the nucleus and the HDEL-mCherry signal of the ER (Figure 4C and Supplemental Figure 7D and 7E). Most of the O3-GFP proteins were relocated to the nucleus under ER stress after 2 h of treatment with dithiothreitol (Figure 4C). The GFP signals of a fusion protein containing truncated O3 without a TMD and the subsequent C-terminal region ($O3^{1–240aa}$-GFP) showed the typical nuclear localization pattern. By contrast, the GFP signals of the fusion protein without the O3 N-terminal region containing the bZIP DNA-binding domain ($O3^{241–568aa}$-GFP) were observed in the ER (Supplemental Figure 7F). These results suggest that O3 is a transmembrane bZIP TF with an ER and nucleus dual-localization signal that can be relocated to the nucleus under ER stress. Similar results have been reported for OsbZIP39 and OsbZIP50, homologous

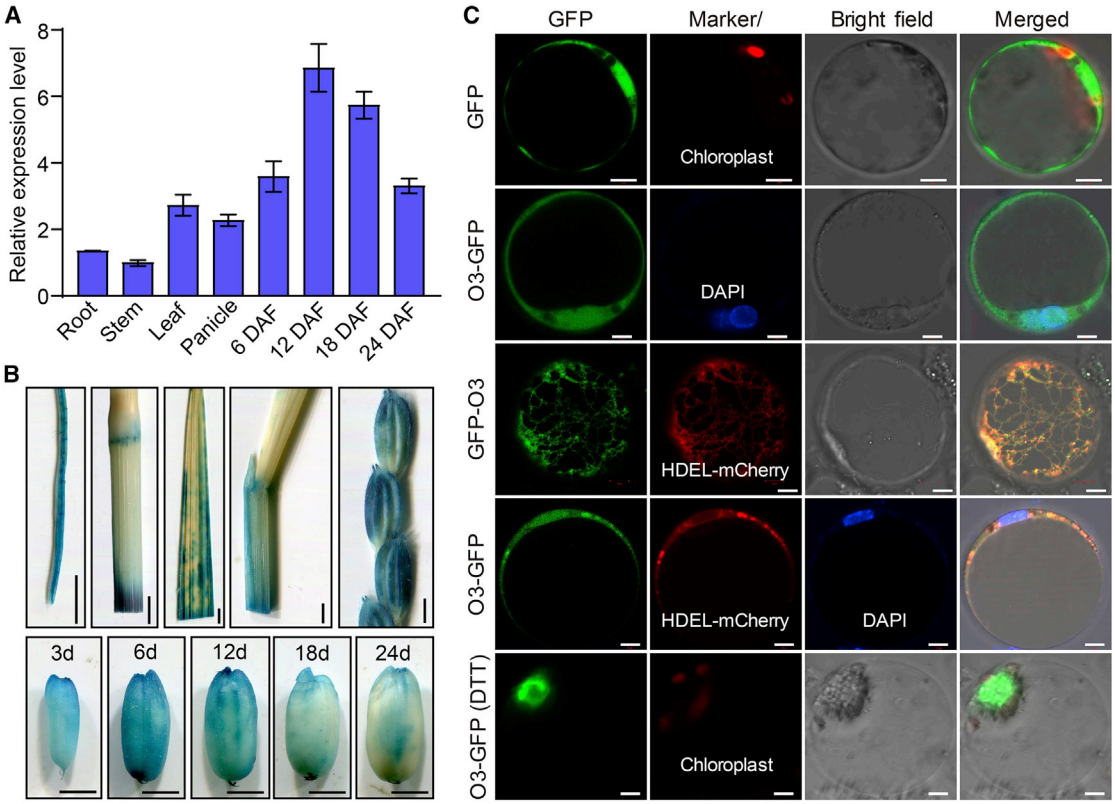

Figure 4. Expression pattern and subcellular localization of O3.

(A) *O3* expression levels in various tissues and in developing endosperm at 6, 12, 18, and 24 DAF. Values are means ± SD from three biological replicates.

(B) GUS staining in roots, stems, leaves, leaf sheaths, spikelets, and developing grains (3, 6, 12, 18, and 24 DAF) driven by the *O3* promoter. Scale bars, 2 mm.

(C) Subcellular localization of O3. Free green fluorescent protein (GFP) and the full-length O3 fusion protein (O3-GFP or GFP-O3) were transiently expressed in rice protoplasts. O3-GFP or GFP-O3 co-localized with DAPI and HDEL-mCherry signals of the nucleus and ER, respectively. O3-GFP was mostly expressed in the nucleus after 2 h of dithiothreitol (DTT) treatment. GFP signals, various organelle marker signals, bright-field images, and merged images of GFP and marker signals are shown in each panel. Scale bars, 5 μm.

bZIP TFs in rice that can be cleaved and transferred from the ER to the nucleus under ER stress (Hayashi et al., 2012; Takahashi et al., 2012).

O3 regulates ER protein-processing genes, and *OsBiP1* OE partly rescues the phenotype of *o3*

We used an RNA sequencing (RNA-seq)-based transcriptome analysis of 12-DAF grains to clarify the function of *O3* in the regulation of endosperm development. A total of 810 and 665 genes were significantly up- and downregulated in *o3*, respectively (Supplemental Data 1). Gene Ontology analysis showed that the differentially expressed genes (DEGs) were mainly involved in protein processing in the ER, protein export, and starch and sucrose metabolism (Supplemental Figure 8A and 8B). Many ER lumen-localized chaperones and associated genes, such as *BIPs*, *PDILs*, *OsFes1C*, *OsErо1*, and *OsSarld*, were upregulated in *o3* endosperm (Supplemental Figures 8C and 10A), suggesting that ER stress may occur in developing endosperm cells of the *o3* mutant. To determine which DEGs were directly regulated by O3, chromatin immunoprecipitation sequencing (ChIP-seq) was performed (Supplemental Figure 9). A total of 5524 binding sites distributed on 1374 genes were identified (Supplemental Data 2), showing that O3 can bind to the promoters of the chaperone genes *OsBiP1* and *PDIL1-1* (Figure 5A). ChIP-qPCR and an electrophoresis mobility shift assay (EMSA) verified that O3 can directly bind to the unfolded protein response element (pUPRE)-II motif (TGACG) of the *OsBiP1* and *PDIL1-1* promoters (Figure 5B–5D). We used a dual luciferase (LUC) reporter system in rice protoplasts to investigate the difference in transcriptional activation activity between O3 and mutated O3. O3 had strong LUC activity, but the mutated O3 had significantly lower LUC activation (Figure 5E–5G), suggesting that O3 could bind to the promoters of *OsBiP1* and *PDIL1-1* to activate their expression, whereas mutated O3 had significantly lower transactivation activity.

We had access to the *osbip1* and *pdil1-1* mutants in the *indica* 'ZJ100' background. Similar to *o3*, these two mutants had opaque and floury grains and showed 57-kDa proglutelin overaccumulation in the endosperm (Figure 5I and Supplemental Figure 10B–10D). Next, we overexpressed *OsBiP1* and *PDIL1-1* in the *o3* mutant background. The *PDIL1-1* OE lines and excessively overexpressed *OsBiP1* lines (relative expression levels raised ~300–900 times) failed to rescue the opaque endosperm phenotype of the *o3* mutant (Supplemental Figure 10E–10H). However, the grain appearance qualities of moderately overexpressed *OsBiP1* lines (relative expression levels raised ~30–80 times) were considerably

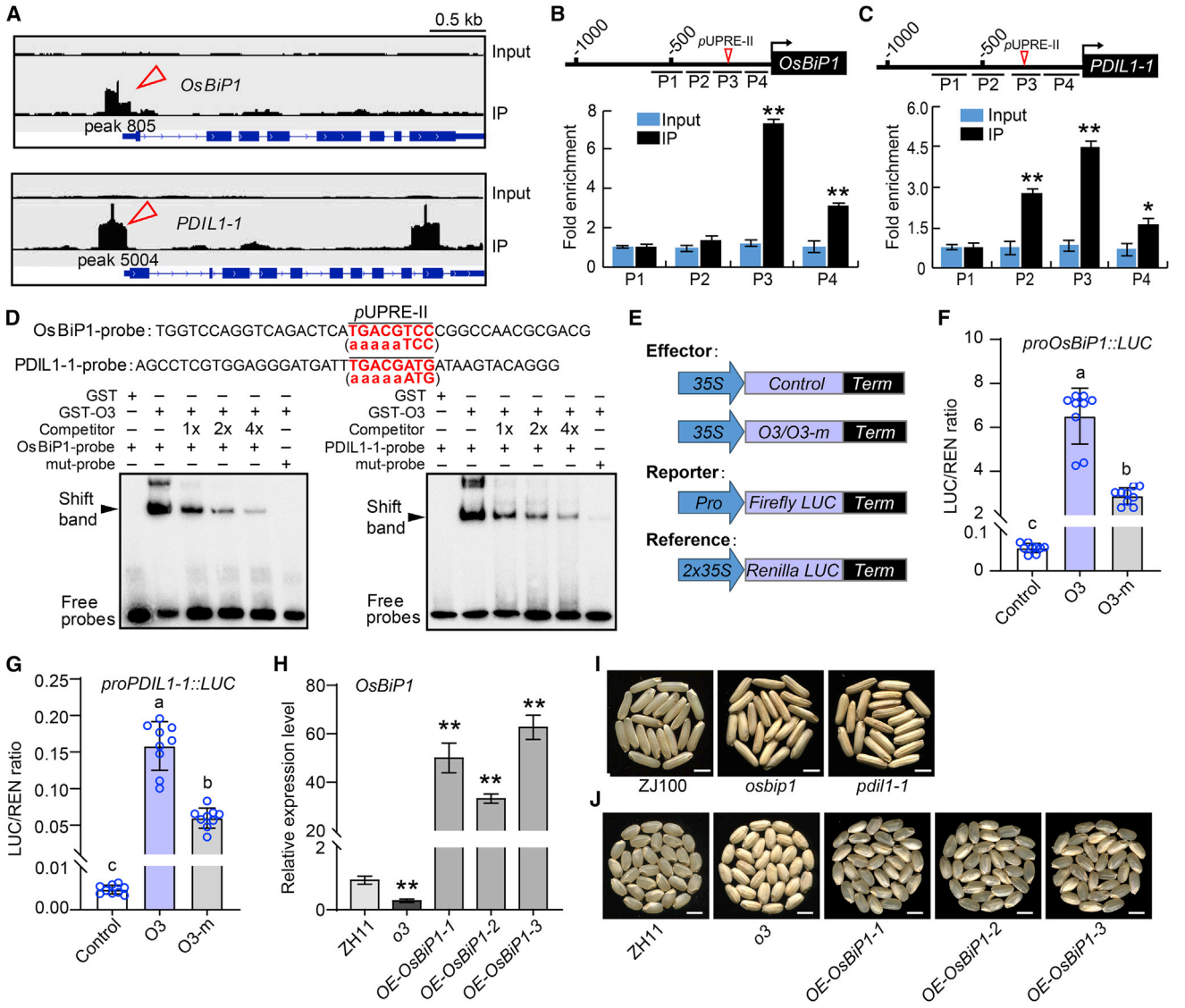

Figure 5. O3 directly binds to the promoters of *OsBIP1* and *PDIL1-1* to activate their transcription.

(A) ChIP-seq results showing the distribution of O3 binding sites for *OsBIP1* and *PDIL1-1* loci, as shown in Integrative Genomics Viewer. Red arrowheads indicate significant peaks calculated by MACS2; positions of peaks are shown in Attachment data II. The input sample was used as a negative control.

(B and C) ChIP-qPCR assay showing the enrichment of O3 at promoter regions of *OsBIP1* **(B)** and *PDIL1-1* **(C)**. DNA samples acquired before immunoprecipitation were used as the input.

(D) EMSA showing that O3 can bind to probes of *OsBIP1* and *PDIL1-1*. The 5-bp consensus pUPRE-II sequence (TGACG) in the promoters of *OsBIP1* and *PDIL1-1* is indicated by red text. The mutated pUPRE-II motif in mut probes is showed in brackets.

(E–G) LUC transient transactivation assay in rice protoplasts. Constructs used in the transient expression assays are shown in **(E)**. O3 significantly activated transcription of *OsBIP1* **(F)** and *PDIL1-1* **(G)**. O3-m represents the mutant form with a Leu-139 to Pro-139 substitution in the coding region.

(H) qRT–PCR analysis of *OsBIP1* transcript level in OE (*OE-OsBIP1*) lines in the *o3* mutant background.

(I) The grain appearance of *osbip1* and *pdil1-1* mutants in the ZhongJian100 (ZJ100) background. Scale bars, 5 mm.

(J) The grain appearance of *OE-OsBIP1* lines in the *o3* background. Scale bars, 5 mm.

Data in **(B)**, **(C)**, and **(F–H)** are means ± SD from at least three biological replicates. Statistically significant differences were determined using Student's *t*-test (indicated by different lowercase letters ($P < 0.05$); $^{*}P < 0.05$, $^{**}P < 0.01$).

improved: many grains showed a transparent endosperm phenotype similar to the wild type (Figure 5H and 5J and Supplemental Figure 10G and 10H), and the expression levels of genes related to ER stress and starch and protein biosynthesis had returned to approximately wild-type levels in moderately over-expressed *OsBiP1* lines (Supplemental Figure 10I and 10J). These results suggest that O3 plays an important role in response to ER stress and regulation of ER protein processing and export by activating the expression of *OsBIP1* and *PDIL1-1*.

O3 directly regulates genes involved in starch and storage protein biosynthesis

Transcriptome analysis and qRT–PCR showed that the expression levels of many starch and storage protein biosynthesis-related

genes were also significantly downregulated in developing endosperm of *o3* (Supplemental Figures 8C and 11A). ChIP-seq, yeast one-hybrid, and dual-LUC reporter assays showed that O3 can directly target and activate the endosperm starch synthesis-associated genes *GBSS1*, *AGPL2*, *SBEI*, and *ISA2* (Supplemental Figure 11B–11D). EMSA confirmed that O3 can directly bind to the GCN4 and CCGTCC motifs in the promoter of *GBSSI* (Supplemental Figure 11E). qRT–PCR analysis showed that the storage protein synthesis-related genes *OsGluA2*, *Prol14*, and *Glb* were dramatically downregulated in the developing endosperm of the *o3* mutant (Supplemental Figures 8C and 12A). A dual-LUC reporter assay showed that O3 can directly target the promoters and activate expression of *OsGluA2*, *Prol14*, and *Glb* in rice protoplasts (Supplemental Figure 12B). EMSA confirmed that O3 can directly bind to the O2 motif in the promoter of *OsGluA2* (Supplemental Figure 12C). These results show that O3 directly participates in regulation of endosperm starch and storage protein biosynthesis, thus regulating the grain yield and quality of rice.

The *o3* mutant is more susceptible to ER stress under high-temperature conditions

High temperatures during the rice grain-filling stage are known to induce ER stress (Howell, 2013). We found that expression of *O3* and its homologous gene *OsbZIP50* increased when seedlings were moved to high temperature (42°C) from normal temperature (28°C) (Supplemental Figure 13A). We next grew wild-type and *o3* plants under field conditions until flowering and then moved the plants to artificial high temperature (35°C, 12 h light/28°C, 12 h dark) and normal temperature (28°C, 12 h light/22°C, 12 h dark) conditions. Under high-temperature conditions, mature grains of the wild type were slightly chalky with slightly reduced weight, but mature *o3* grains were very floury and shrunken with significantly reduced size and weight (Figure 6A and 6B and Supplemental Figure 13B). Compared with normal-temperature conditions, the wild type and *o3* mutant had significantly lower amylose and total protein content under high-temperature conditions; however, the differences between conditions were greater for the *o3* mutant than for the wild type (Figure 6C–6E). An SDS-PAGE assay showed that the *o3* mutant had a higher endosperm accumulation of 57-kDa proglutelin and a lower accumulation of 20-kDa basic and 40-kDa acidic subunits of mature glutelins and 13-kDa and 16-kDa prolamin under both normal- and high-temperature conditions; however, differences between the *o3* mutant and the wild type were greater under high-temperature conditions (Figure 6F). These results indicate that endosperm development is more susceptible to heat stress in the *o3* mutant than in the wild type.

We next examined the expression profiles of ER stress-associated genes in the wild type and *o3* mutant under high-temperature and normal-temperature conditions. In the *o3* mutant, genes that responded to ER stress, such as *OsBIPs*, *PDIL1-1*, *OsbZIP50*, *PDIL2-3*, *Calnexin*, *OsFes1*, and *OsEro*, had higher expression levels under high-temperature than under normal-temperature conditions (Figure 6G and Supplemental Figure 13C). Because *OsbZIP50* can be cleaved and transferred from the ER to the nucleus to upregulate expression of chaperone genes under ER stress (Supplemental Figure 14A; Hayashi et al., 2012), we performed a semi-quantitative RT-PCR analysis of *OsbZIP50* transcripts under high-temperature and normal-temperature conditions. *OsbZIP50* mRNA was present in an unspliced (U) form in developing endosperm of the wild type under high-temperature and normal-temperature conditions; however, the spliced (S) form of *OsbZIP50* mRNA was detected in the *o3* mutant, and the S form was more abundant under high-temperature conditions (Figure 6H). This suggests that developing endosperm of the *o3* mutant experienced more severe ER stress than that of the wild type under heat stress. In the wild type, the expression levels of *OsBiP1*, *PDIL1-1*, and *OsbZIP50* were lower under high-temperature conditions than under normal-temperature conditions (Figure 6G and Supplemental Figure 13C), which suggests that O3 participates in maintaining ER homeostasis in developing endosperm of the wild type under heat stress. The expression levels of genes related to storage protein and starch synthesis were lower in developing endosperm of the *o3* mutant under high-temperature conditions compared with normal-temperature conditions, but expression levels of genes related to starch degradation were higher (Supplemental Figure 13D and 13E). These results suggest that *O3* plays an important role in maintaining ER homeostasis and regulating storage substance accumulation and endosperm development under heat stress.

DISCUSSION

O3 affects rice grain filling by simultaneously regulating starch and storage protein biosynthesis

Starch and storage proteins determine the yield and quality of cereal grains. Their biosynthesis in grains requires a series of enzymes that are accurately regulated by a group of spatiotemporally expressed TFs (Kawakatsu et al., 2009; Wang et al., 2013; Bai et al., 2016; Xu et al., 2016; Bello et al., 2019; Xiong et al., 2019). In maize, many TFs have been reported to synergistically regulate starch and protein biosynthesis in endosperm. O2 is an endosperm-specific bZIP TF that mainly regulates expression of the α- and β-*zein* genes by recognizing the O2 box in their promoters. O2 can directly transactivate *PPDK1*, *PPDK2*, *SSIII*, *SUS1*, and *SUS2* to regulate starch biosynthesis and sucrose synthase-mediated endosperm filling (Zhang et al., 2016; Deng et al., 2020). Prolamin-box binding factor (PBF), an endosperm-specific DNA binding with one finger (DOF) TF, can also regulate expression of *zein* genes by recognizing the prolamin-box; it can also interact with O2 and enhance its transcriptional activation activity (Vicente-Carbajosa et al., 1997). ZmNAC128 and ZmNAC130 are homologous and functionally redundant endosperm-specific NAC TFs; they bind to the ACGCAA motif on the promoter of *16-kDa* γ*-zein* and the starch synthesis gene *Bt2* to activate their expression. Simultaneous knockdown of *ZmNAC128* and *ZmNAC130* expression with RNAi causes a shrunken kernel phenotype with significantly reduced starch and protein contents (Zhang et al., 2019b). The upstream regulator ZmABI19 can directly regulate multiple key grain-filling TFs, including *O2*, *PBF1*, *ZmbZIP22*, *NAC130*, *Opaque11*, and *SWEET4c*, by binding to the RY motif in the early endosperm development stage of maize. The kernels of the *zmabi19* mutant are opaque and reduced in size with lower accumulation of zeins, starch, and lipids (Zhang et al., 2021).

Few regulators that can simultaneously regulate starch and protein biosynthesis in rice endosperm have been reported. A bZIP

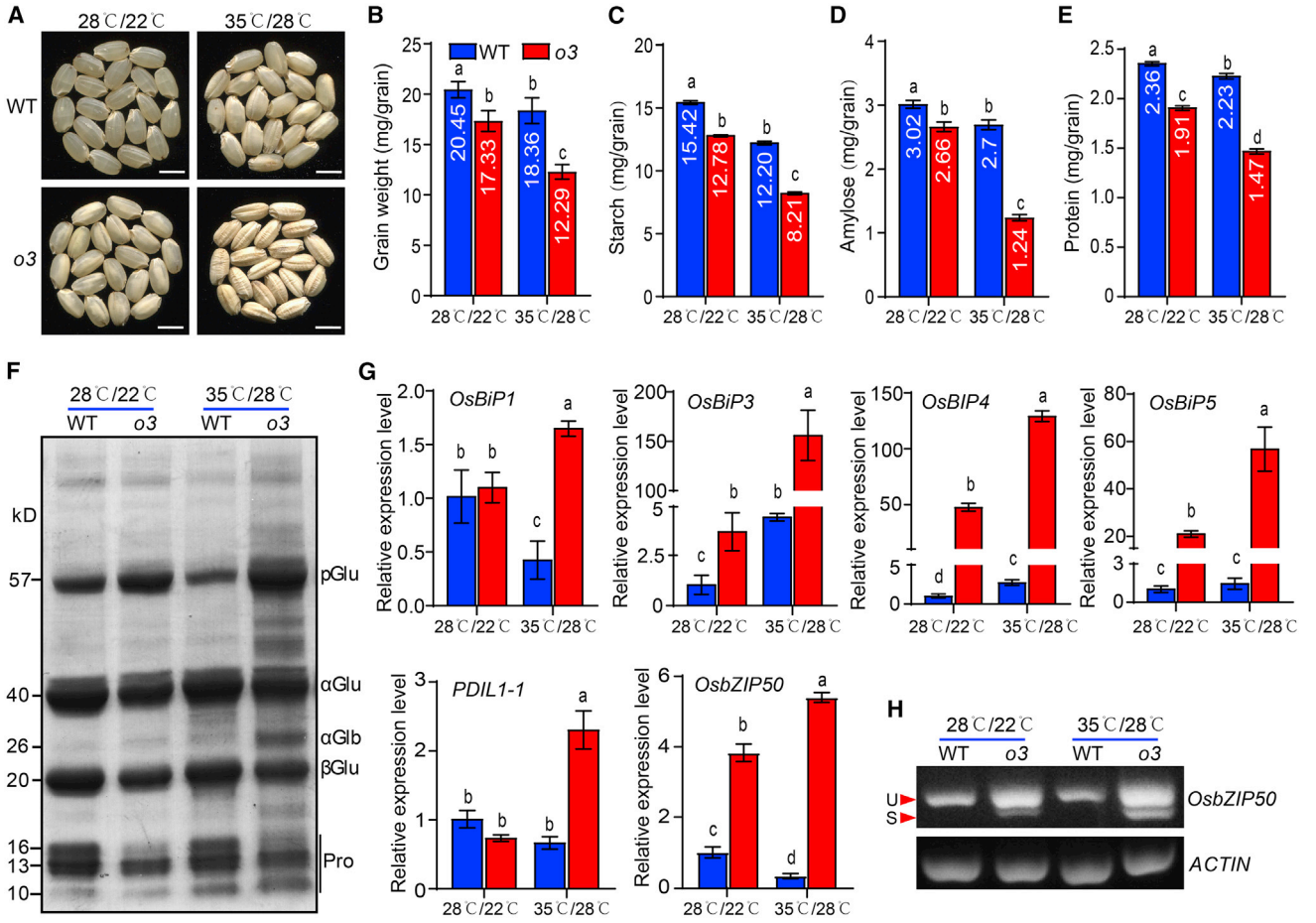

Figure 6. The *o3* mutant is more prone to ER stress under high-temperature conditions.

(A) Appearance of WT and *o3* grains under high-temperature conditions (35°C, 12 h light/28°C, 12 h dark) and normal-temperature conditions (28°C, 12 h light/22°C, 12 h dark). Scale bars, 5 mm.

(B–E) The grain weight **(B)**, total starch content **(C)**, amylose content **(D)**, and total protein content **(E)** of WT and *o3* grains under high- and normal-temperature conditions.

(F) SDS-PAGE profiles of total storage proteins of WT and *o3* dry grains.

(G) Transcript levels of genes related to ER stress in WT and *o3* grains at 9 DAF under high- and normal-temperature conditions.

(H) Semi-quantitative PCR analysis of *OsbZIP50* transcripts in WT and *o3* endosperm cells under high- and normal-temperature conditions. U and S, the unspliced and spliced forms of the *OsbZIP50* mRNA, respectively.

Data in **(B–E)** and **(G)** are means ± SD from at least three biological replicates. Significant differences are indicated by different letters according to Student's *t*-test.

TF homolog of maize O2, OsbZIP58, has been reported to regulate both starch and storage protein biosynthesis (Kawakatsu et al., 2009; Wang et al., 2013). The rice NAC TFs OsNAC20 and OsNAC26, orthologs of maize ZmNAC128 and ZmNAC130, respectively, also play an essential role in regulation of starch and storage protein synthesis by directly transactivating expression of *SSI*, *Pul*, *GluA1*, *GluB4/5*, *α-globulin*, and *16-kDa prolamin*, and the *osnac20/26* double mutant has floury seeds with significantly lower starch and storage protein contents (Wang et al., 2020). In this study, we identified the rice opaque endosperm mutant *o3*. *O3* encodes a transmembrane bZIP TF, OsbZIP60 (Figure 3 and Supplemental Figure 7A–7C; Yang et al., 2022). ChIP-seq and LUC assays demonstrated that O3 could directly bind to the promoters and activate the expression of the starch synthesis-related genes *GBSSI*, *AGPL2*, *SBEI*, and *ISA2* as well as the storage protein synthesis-related genes *OsGluA2*, *Prol14*, and *Glb1* (Supplemental Figures 8, 11, and 12). The expression levels of these starch and storage protein synthesis-related genes were significantly downregulated in the *o3* mutant, which may lead to the lower starch content, protein content, and grain weight of the *o3* mutant. This also resulted in alterations of starch fine structure, such as amylopectin chain length distributions and developmental defects of compound starch grains in the endosperm of *o3* compared with the wild type (Figures 1H–1J and 2J–2O and Supplemental Figures 2 and 3). EMSA further clarified that O3 directly binds to the GCN4 (TGA(G/C)TCA) and CCGTCC motifs in the *GBSSI* promoter and the O2 motif (GATGACATAG) in the *OsGluA2* promoter (Supplemental Figures 11 and 12). In maize, the O2 motif (TGACGTGGC) is the key element for regulation of zein and starch synthesis-related genes (Zhang et al., 2016; Deng et al., 2020). Therefore, we believe that the O2 motif is the core element for regulation of starch and storage protein-related gene expression by bZIP TFs in maize and rice. O3 (OsbZIP60)

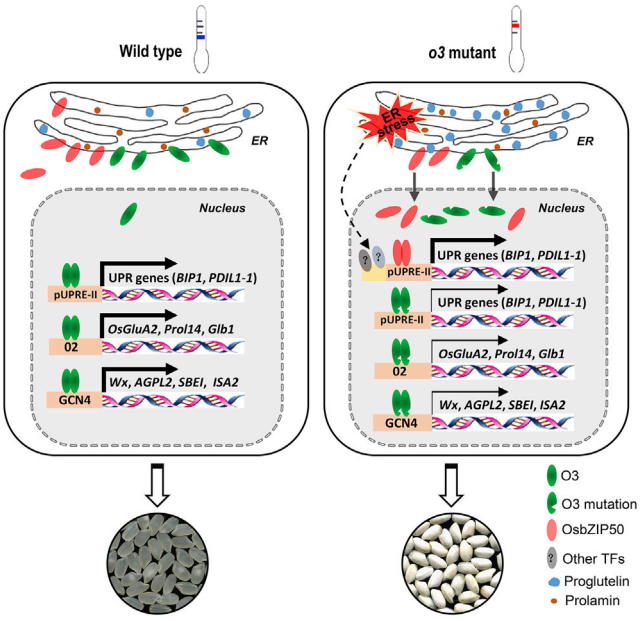

Figure 7. Proposed model of the role of O3 in maintaining ER homeostasis and regulating endosperm storage protein and starch biosynthesis in rice.

Under normal conditions in the WT, O3 is located in the ER and the nucleus. It simultaneously regulates ER protein processes and secretion as well as storage protein and starch biosynthesis in endosperm cells by binding to specific motifs, such as pUPRE-II, O2, and the GCN4 box, to activate transcription of UPR genes and storage protein and starch biosynthesis genes, ultimately ensuring normal development of rice grains. However, mutation of O3 leads to downregulated expression of ER stress-related genes, such as *OsBIP1* and *PDIL1-1*, as well as genes related to storage protein and starch biosynthesis, resulting in ER stress and an impaired protein folding process in the ER. This leads to excessive accumulation of the 57-kDa glutelin precursor and reduces the contents of starch and storage proteins. High temperature can aggravate ER stress and lead to more abnormal grain development in the *o3* mutant. As physiological feedback, more O3 (mutated) is transferred to the nucleus from the ER, together with OsbZIP50 and other unknown TFs, to activate expression of key UPR genes to maintain ER homeostasis, especially under high-temperature conditions.

can form homodimers (Hayashi et al., 2013). These results suggest that O3 is the core regulatory factor in rice endosperm development; it can simultaneously regulate biosynthesis of endosperm starch and storage protein, thus affecting rice quality and grain yield, similar to maize O2 (Figure 7; Zhang et al., 2016; Deng et al., 2020).

O3 plays an important role in protein processing and export in the ER of rice endosperm cells

Rice grain storage proteins are initially synthesized on the ER membrane and translocated into the ER lumen in endosperm cells. They are then stored as morphologically distinct protein bodies in different subcellular compartments (Yamagata et al., 1982). Prolamins are stored as intracisternal inclusion granules within the ER lumen and bud off from the ER to form PBIs. Glutelins are synthesized as 57-kDa precursors on the rough ER and are transported to PSVs to be cleaved into mature acidic and alkaline subunits to form PBII by the DV-mediated post-Golgi apparatus trafficking pathway or ER-derived precursor accumulating compartments that bypass the Golgi apparatus (Krishnan et al., 1986; Takahashi et al., 2005). Mutations in the key genes that regulate storage protein folding, processing, and transport lead to 57-kDa proglutelin overaccumulation (57H) in endosperm cells. The *esp2* mutants, resulting from knockout of ER-localized PDIL1-1, develop many ER-derived, small, PBI-like vesicles containing cross-linked glutelins and prolamins in developing endosperm (Takemoto et al., 2002; Han et al., 2012). Other rice 57H mutants, such as *rab5a*, *vps9a*, *gpa3*, *gpa5*, *osnhx5*, and *calcium caffeine zinc1*, are defective in post-Golgi apparatus trafficking and produce many abnormal protein granules and paramural body structures at the apoplast (Wang et al., 2010; Liu et al., 2013; Zhu et al., 2019; Ren et al., 2020; Pan et al., 2021). OsVPE1 is responsible for processing and maturation of glutelins in PSV, and the *osvpe1* mutants develop many round PBIIs (Wang et al., 2009).

In this study, we found that mutation of *O3* caused overaccumulation of 57-kDa proglutelins and significantly lower accumulation of mature 20-kDa basic and 40-kDa acidic subunits. 13-kDa and 16-kDa prolamins were also notably decreased in the *o3* mutant compared with the wild type (Figure 1M). Cytological studies showed that many protein bodies were retained in the ER lumen of *o3*, similar to the small PBI-like vesicles observed in the *pdil1-1* mutant (Takemoto et al., 2002). Many ER-derived vesicles with or without protein bodies were observed in endosperm cells of the *o3* mutant (Figure 2D–2F). The ER-derived vesicles containing protein bodies have certain similarities to the aberrant vesicle structures in the *gpa4* mutant (Wang et al., 2016). These results demonstrate that grain storage protein processing and export in the ER were disturbed in *o3* endosperm cells. In addition to directly binding and activating genes related to starch and storage protein biosynthesis, O3 also activated expression of *OsBIP1* and *PDIL1-1* (Figure 5A–5G), two major chaperones that assist with folding of immature secretory proteins in the ER. Therefore, the protein folding and processing system in the ER may be impaired in the *o3* mutant, causing unfolded protein accumulation and production of abnormal protein body structures in endosperm cells. Otherwise, the vesicle structures that contain protein bodies in *o3* endosperm cells may be precursor accumulating compartment vesicles formed by expansion of the terminal of rough ER containing glutelin precursors. These results show that O3 plays an important role in protein processing and export in the ER of rice endosperm cells.

O3 is essential for maintaining ER homeostasis in rice endosperm cells under heat stress

RNA-seq analysis showed that many UPR genes related to protein folding and processing were upregulated in the *o3* mutant (Supplemental Figure 8), indicating that the *o3* mutant experiences ER stress. Subcellular localization assays revealed that O3 is localized in the ER and nucleus under normal conditions. Under ER stress conditions, O3 was mostly transferred to the nucleus (Figure 4C and Supplemental Figure 7). O3 can directly bind to the promoters and activate the expression of *OsBIP1* and *PDIL1-1*. However, the expression level and protein abundance of *OsBIP1* and *PDIL1-1*, as well as the expression levels of many UPR genes, were significantly upregulated in the *o3* mutant (Figure 1N and Supplemental Figures 8

and 10). This result suggests that there may be physiological feedback; to maintain ER homeostasis in *o3* mutants, the expression levels of genes related to protein folding and processing were upregulated (Figure 7). The *pdil1-1* and *osbip1* mutants show an opaque endosperm phenotype similar to that of *o3* (Han et al., 2012; Supplemental Figure 10C). Moderate OE of *OsBIP1* in the *o3* mutant could cause expression levels of genes related to ER stress and starch and protein biosynthesis to return to approximately wild-type levels, thus partly restoring the transparent endosperm phenotype; by contrast, excessive overexpression of *OsBiP1* and OE of *PDIL1-1* failed to rescue the *o3* phenotype (Figure 5H–5J and Supplemental Figure 10E–10J). These results indicate that O3 plays an important role in maintaining ER homeostasis by activating the key stress response gene *OsBIP1* rather than *PDIL1-1*. *OsbZIP50*, a homolog of *O3*, is a well-known regulator specifically responsive to ER stress. Under ER stress conditions, unconventional splicing of *OsbZIP50* mRNA occurs, and the shorter OsbZIP50 protein is relocated to the nucleus to activate expression of UPR genes (Supplemental Figure 14A; Hayashi et al., 2012). We found that *OsbZIP50* was present mainly in the U form in the wild type. However, *OsbZIP50* was significantly upregulated and occurred in the S form in the *o3* mutant (Figure 6G and 6H and Supplemental Figure 14B). We found that the TMD of O3 was responsible for its ER localization (Figure 4C and Supplemental Figure 7), whereas semi-quantitative RT-PCR analysis showed that the *O3* mRNA did not have alternative splicing in developing endosperm, which suggested that the TMD of O3 may be cleaved by protease under ER stress, consistent with *Arabidopsis* AtbZIP17 and AtbZIP28 (Supplemental Figure 14B; Iwata et al., 2017). A LUC reporter assay showed that OsbZIP50 can enhance transient transactivation of *OsBIP1* and *PDIL1-1* together with O3 in rice protoplasts (Supplemental Figure 14C). This suggests that *OsbZIP50* activates UPR genes related to protein folding to help maintain ER homeostasis in the *o3* mutant (Figure 7).

High temperatures during the rice grain-filling stage can induce ER stress and lead to grain chalkiness (Howell, 2013; Ren et al., 2021). We found that the *o3* mutant was more sensitive to high-temperature stress than the wild type (Figure 6A–6E). Genes that respond to ER stress, such as *OsBIPs*, *PDILs*, *Erdj3B*, *Calnexin*, *OsFes1*, and *OsEro1*, were significantly upregulated in the *o3* mutant under high-temperature compared with normal-temperature conditions (Figure 6G and Supplemental Figure 13C). These results indicate that high-temperature conditions induce higher levels of ER stress in the endosperm cells of the *o3* mutant. *OsbZIP50* was also significantly upregulated with higher accumulation of the S form in the *o3* mutants compared with normal-temperature conditions (Figure 6G and 6H). Although the transcriptional activation function of mutated O3 was weaker, its target genes, *OsBIPs* and *PDIL1-1*, and other UPR genes were upregulated rather than downregulated in the *o3* mutant (Supplemental Figures 8 and 10 and Figure 6G). It is possible that these genes were activated by OsbZIP50 and other TFs induced by ER stress to maintain ER homeostasis in endosperm cells of the *o3* mutant, especially under high-temperature conditions (Figure 7 and Supplemental Figure 14C). The expression levels of genes related to storage protein and starch biosynthesis were lower, but those of genes related to starch degradation were higher in developing endosperm of the *o3* mutant under high-temperature conditions compared with normal-temperature conditions (Supplemental Figure 13D and 13E), which presumably led to the more pronounced abnormal grain phenotype of the *o3* mutant under high-temperature conditions (Figure 7). These results suggest that O3 is essential for maintaining ER homeostasis in endosperm cells under heat stress. Our research indicates that rice O3 (OsbZIP60) participates simultaneously in regulating storage protein and starch biosynthesis and maintaining ER homeostasis in grain endosperm and therefore plays a central role in rice grain development. Our study provides useful information for potential genetic improvement of yield and grain quality in rice.

METHODS

Plant materials and growth conditions

The *o3* mutant was identified from an ethyl methanesulfonate-induced mutant pool of *japonica* rice 'Zhonghua11' (ZH11). Two F_2 populations from the crosses of *o3* × Nanjing11 (*indica*) and *o3* × ZH11 were used to map the mutant gene. All plants used in this study were grown in paddy fields in Hangzhou, Zhejiang Province, China, during the normal growing seasons. At the flowering stage, some well-grown wild-type and *o3* plants were moved to plant growth chambers under normal-temperature (28°C, 12 h light/22°C, 12 h dark) and high-temperature (35°C, 12 h light/28°C, 12 h dark) conditions.

Microscopy analysis

To observe starch grain and protein body development, transverse sections of wild-type and *o3* endosperm at 9 DAF were used to prepare semi-thin sections (0.5 μm). Samples were stained with I_2–KI or Coomassie brilliant blue for 5 s and subsequently examined under a light microscope. The brown rice was cut transversely to prepare samples for scanning electron microscopy analysis. Images were obtained with an S3400N scanning electron microscope (Hitachi, Tokyo, Japan). To observe the ultrastructure of amyloplasts, PBI, and PBII, 6–12-DAF grains were observed with a transmission electron microscope.

SDS-PAGE and immunoblot analysis

SDS-PAGE analysis was performed as described by Ren et al. (2014). In brief, total dry grain proteins were extracted using an extraction buffer. The proteins were resolved by SDS-PAGE on a 4%–20% (w/v) graded gel, followed by Coomassie brilliant blue staining and photography. For immunoblotting, fresh rice grains were used for protein extraction. Total proteins were then separated on 10% SDS-PAGE gels and immunoblotted with specific antibodies. The specific bands were detected using an enhanced chemiluminescence detection kit (Thermo Fisher Scientific).

Analyses of physicochemical properties of endosperm starch

The total starch and amylose content was measured using a starch assay kit (Megazyme, Wicklow, Ireland). Lipid and total protein contents in the grains were measured according to the method described by Kang et al. (2005). The glutelin, prolamin, globulin, and albumin in the mature endosperm (milled rice) were extracted and measured according to the methods described by Yang et al. (2015) and Kang et al. (2005). To determine the starch pasting properties, 3 g of milled rice powder was transferred to a container with 25 mL of distilled water. The sample was mixed and measured with a Rapid Visco Analyzer (Newport Scientific, Narrabeen, NSW, Australia). To determine the chain length distribution of amylopectin, 5 mg of rice flour was digested with isoamylase and then analyzed by capillary electrophoresis.

Mapping of the *O3* gene

To map the *O3* locus, 207 individuals with opaque endosperm were selected from the F_2 population derived from *o3* × NJ11. Polymorphic

simple sequence repeats (SSR) markers were selected to link to *O3*. Next, the MutMap method was used to map *O3* according to the description in Abe et al. (2012). A recessive pool containing 40 individuals with opaque endosperm was selected from the F_2 population derived from *o3* × ZH11; ZH11 was the dominant pool. Both bulked DNA samples were subjected to whole-genome sequencing using the Illumina HiSeq PE150 platform (Novogene, Beijing, China). The short reads were aligned to the Nipponbare reference sequence to enable identification of reliable SNPs. The regression lines of SNP index plots were generated by averaging scores in a sliding 2-Mb window with 10-kb increments. Candidate SNPs with a SNP index greater than 0.8 from the mutagenesis were screened further. The primers used for mapping are listed in Supplemental Table 1.

Vector construction and plant transformation

To create the complementation vector, the *O3* genomic fragment, including its native promoter, was amplified from ZH11 and cloned into the binary expression vector pCAMBIA1300. The *O3* cDNA sequence driven by the *UBIQUTIN1* promoter was cloned into the binary vectors pCAMBIA1390 and pRHVnGFP to generate OE vectors. To knock out *O3* using the CRISPR-Cas9 system, single guide RNAs targeting sites were constructed into the BGK03 vector (Biogle, Hangzhou, China). Complementation and OE vectors were transformed into *o3*, and the CRISPR-Cas9 vectors were transformed into ZH11. Sequences of the primers used for vector construction and detection are listed in Supplemental Table 1.

RNA-seq and qRT–PCR analysis

For transcriptome analysis, total RNA samples from wild-type and *o3* grains at 9 DAF were sequenced on the HiSeq 4000 platform (Illumina) by Novogene Technology (Beijing, China) to obtain clean reads. DEGs were identified by a false discovery rate $\leq$0.05 and an absolute value of the $\log_2$ ratio $\geq$1. Gene Ontology enrichment analysis was performed based on the hypergeometric distribution using R. Pathway analysis was performed in MapMan (https://mapman.gabipd.org/) by searching against the *Oryza sativa* TIGR7 database.

Total RNA was extracted from different plant tissues using the TRIzol reagent (Invitrogen, Carlsbad, CA, USA). RNA was reverse transcribed into cDNA using a ReverTra Ace qPCR RT Kit (Toyobo, Osaka, Japan). qPCR was performed using SYBR Green Real-Time PCR Master Mix (Toyobo). The rice *Ubiquitin* gene (Os03g0234200) was used as an internal control. The primer sequences used in this analysis are listed in Supplemental Table 1.

Transcriptional activity, yeast one-hybrid, and LUC activity assays

To test the transactivation activity of O3, the coding sequence (CDS) of *O3* was amplified from ZH11, cloned into the pGBKT7 vector, and transformed into yeast strain AH109. The transformed yeast strains were examined on SD/-Trp and SD/-Trp/-His/-Ade/X-α-GAL plates for 4 days at 30°C. For the yeast one-hybrid assay, the CDS of *O3* was cloned into the pB42AD vector, and the promoter regions of *GBSS1*, *AGPL2*, *SBE1*, and *ISA2* were cloned into the pLacZi2μ vector. Bait and prey plasmids were co-transformed into yeast EGY48. The assay was performed using the Clontech Yeast One-Hybrid System (Takara, Beijing, China) following the manufacturer's instructions.

For the LUC activity assay, the promoter regions of *GBSS1*, *AGPL2*, *SBEI*, *ISA2*, *OsGluA2*, *Prol14*, and *Glb1* were inserted into the 190LUC vector as reporters. The coding sequences of *O3* and the *O3* mutant form (O3-m) were inserted into the expression vector as effectors. The LUC activity assay was then performed as described by Wang et al. (2020). The primers used in this assay are listed in Supplemental Table 1.

Subcellular localization of O3 and OsbZIP50

To verify the subcellular localization of O3 and OsbZIP50, coding regions without a termination codon were cloned into the pAN580 and pCAMBIA1305-GFP vectors. The fusion of GFP and different truncated forms of O3 together with marker vectors (HDEL-mCherry, D53-mCherry, GHD7-CFP, and PHT4-RFP) were co-transformed into rice protoplasts. DAPI was used as a nuclear marker. The pCAMBIA1305-O3-GFP vector was infiltrated into 3-week-old leaf epidermal cells of tobacco via *Agrobacterium*.

ChIP-seq and ChIP-qPCR

ChIP assays were performed following a method described previously with slight modifications (Xiong et al., 2019). In brief, 9-DAF endosperm was harvested from the GFP-O3 OE lines in the *o3* background and cross-linked in 1% formaldehyde. The cross-linked endosperm was dried and ground into powder in liquid N_2, followed by nuclear isolation and sonication. Protein A and G agarose beads (Beyotime, Shanghai, China) and a GFP antibody were used to precipitate the protein and DNA complex, which was digested by Proteinase K and recovered using a PCR purification kit. DNA samples acquired without immunoprecipitation by the GFP antibody were used as the input. The immunoprecipitated DNA and input DNA were sequenced on the HiSeq 2500 platform (Novogene, Beijing, China). ChIP-seq raw sequencing data were mapped to the rice reference genome using the Burrows–Wheeler Alignment tool. Model-based analysis of ChIP-seq data 2 (MACS2) was used for peak calling, and significantly enriched peaks (binding sites) were identified using a corrected *P* value of less than 0.05 in the IP libraries compared with input DNA (Supplemental Data 2). Visual analysis was performed using Integrative Genomics Viewer (v.2.3.26). To validate the specific regions of target genes bound by O3, the immunoprecipitated DNA and input DNA were used in ChIP-qPCR analysis. The enrichment value of each fragment was normalized to that of the input sample. The primers used in this assay are listed in Supplemental Table 1.

EMSA

The GST-O3$^{104–176aa}$ protein containing the bZIP domain structure was purified. The EMSA probes of *BIP1*, *PDIL1-1*, *GBSS1*, and *OsGluA2* were commercially synthesized and labeled using the EMSA Probe Biotin Labeling Kit (Beyotime, Shanghai, China), and non-labeled probes were used as competitors. Probe sequences are listed in Supplemental Table 1. The DNA binding reaction was performed for 20 min at 25°C, and the products were then electrophoresed using 6% acrylamide gels. The DNA probes were transferred to a nylon membrane. Finally, the oligo bands were detected using the LightShift Chemiluminescent EMSA Kit and streptavidin-horseradish peroxidase (Beyotime).

SUPPLEMENTAL INFORMATION

Supplemental information is available at *Plant Communications Online*.

FUNDING

This work was supported by the National Natural Science Foundation of China (31971925 and 32172080), the Natural Science Foundation of Zhejiang Province (LR20C13002), the Special Support Plan for High-Level Talents in Zhejiang Province (2019R52032), and the International Science & Technology Innovation Program of the Chinese Academy of Agricultural Sciences, China (CAAS-ZDRW202109).

AUTHOR CONTRIBUTIONS

X.W. and R.C. designed experiments and analyzed data. R.C., S.Z., G.J., Y.D., L.M., N.D., F.L., M.Z., G.S., S.H., Z.S., and S.T. performed the experiments. R.C., X.W., and J.Z. wrote the manuscript and prepared the illustrations. X.W. and P.H. conceived the idea and supervised the project. All authors read and approved the final manuscript.

ACKNOWLEDGMENTS

We thank Prof. Jianmin Wan for providing the antibodies for PDIL1-1, OsBiP1, OsGluA, OsGluB, and Globulin. No conflict of interest is declared.

Received: June 8, 2022
Revised: September 30, 2022
Accepted: October 14, 2022
Published: November 14, 2022

REFERENCES

Abe, A., Kosugi, S., Yoshida, K., Natsume, S., Takagi, H., Kanzaki, H., Matsumura, H., Yoshida, K., Mitsuoka, C., Tamiru, M., et al. (2012). Genome sequencing reveals agronomically important loci in rice using MutMap. Nat. Biotechnol. **30**:174–178.

Bai, A.N., Lu, X.D., Li, D.Q., Liu, J.X., and Liu, C.M. (2016). NF-YB1-regulated expression of sucrose transporters in aleurone facilitates sugar loading to rice endosperm. Cell Res. **26**:384–388.

Ball, S.G., and Morell, M.K. (2003). From bacterial glycogen to starch: understanding the biogenesis of the plant starch granule. Annu. Rev. Plant Biol. **54**:207–233.

Beckles, D.M., Smith, A.M., and ap Rees, T. (2001). A cytosolic ADP-glucose pyrophosphorylase is a feature of graminaceous endosperms, but not of other starch-storing organs. Plant Physiol. **125**:818–827.

Bello, B.K., Hou, Y., Zhao, J., Jiao, G., Wu, Y., Li, Z., Wang, Y., Tong, X., Wang, W., Yuan, W., et al. (2019). NF-YB1-YC12-bHLH144 complex directly activates Wx to regulate grain quality in rice (Oryza sativa L.). Plant Biotechnol. J. **17**:1222–1235.

Bertolotti, A., Zhang, Y., Hendershot, L.M., Harding, H.P., and Ron, D. (2000). Dynamic interaction of BiP and ER stress transducers in the unfolded-protein response. Nat. Cell Biol. **2**:326–332.

Deng, Y., Humbert, S., Liu, J.X., Srivastava, R., Rothstein, S.J., and Howell, S.H. (2011). Heat induces the splicing by IRE1 of a mRNA encoding a transcription factor involved in the unfolded protein response in Arabidopsis. Proc. Natl. Acad. Sci. USA. **108**:7247–7252.

Deng, Y., Wang, J., Zhang, Z., and Wu, Y. (2020). Transactivation of Sus1 and Sus2 by Opaque2 is an essential supplement to sucrose synthase-mediated endosperm filling in maize. Plant Biotechnol. J. **18**:1897–1907.

Fu, F.F., and Xue, H.W. (2010). Co-expression analysis identifies Rice Starch Regulator1, a rice AP2/EREBP family transcription factor, as a novel rice starch biosynthesis regulator. Plant Physiol. **154**:927–938.

Han, X., Wang, Y., Liu, X., Jiang, L., Ren, Y., Liu, F., Peng, C., Li, J., Jin, X., Wu, F., et al. (2012). The failure to express a protein disulphide isomerase-like protein results in a floury endosperm and an endoplasmic reticulum stress response in rice. J. Exp. Bot. **63**:121–130.

Hayashi, S., Takahashi, H., Wakasa, Y., Kawakatsu, T., and Takaiwa, F. (2013). Identification of a cis-element that mediates multiple pathways of the endoplasmic reticulum stress response in rice. Plant J. **74**:248–257.

Hayashi, S., Wakasa, Y., Takahashi, H., Kawakatsu, T., and Takaiwa, F. (2012). Signal transduction by IRE1-mediated splicing of bZIP50 and other stress sensors in the endoplasmic reticulum stress response of rice. Plant J. **69**:946–956.

Howell, S.H. (2013). Endoplasmic reticulum stress responses in plants. Annu. Rev. Plant Biol. **64**:477–499.

Iwata, Y., Ashida, M., Hasegawa, C., Tabara, K., Mishiba, K.I., and Koizumi, N. (2017). Activation of the Arabidopsis membrane-bound transcription factor bZIP28 is mediated by site-2 protease, but not site-1 protease. Plant J. **91**:408–415.

Iwata, Y., and Koizumi, N. (2005). An Arabidopsis transcription factor, AtbZIP60, regulates the endoplasmic reticulum stress response in a manner unique to plants. Proc. Natl. Acad. Sci. USA. **102**:5280–5285.

Kang, H.G., Park, S., Matsuoka, M., and An, G. (2005). White-core endosperm floury endosperm-4 in rice is generated by knockout mutations in the C-type pyruvate orthophosphate dikinase gene (OsPPDKB). Plant J. **42**:901–911.

Kawakatsu, T., Yamamoto, M.P., Touno, S.M., Yasuda, H., and Takaiwa, F. (2009). Compensation and interaction between RISBZ1 and RPBF during grain filling in rice. Plant J. **59**:908–920.

Krishnan, H.B., and Okita, T.W. (1986). Structural Relationship among the Rice Glutelin Polypeptides. Plant Physiol **81**:748–753.

Li, X., Wu, Y., Zhang, D.Z., Gillikin, J.W., Boston, R.S., Franceschi, V.R., and Okita, T.W. (1993). Rice prolamine protein body biogenesis: a BiP-mediated process. Science **262**:1054–1056.

Liu, F., Ren, Y., Wang, Y., Peng, C., Zhou, K., Lv, J., Guo, X., Zhang, X., Zhong, M., Zhao, S., et al. (2013). OsVPS9A functions cooperatively with OsRAB5Ato regulate post-Golgi dense vesicle-mediated storage protein trafficking to the protein storage vacuole in rice endosperm cells. Mol. Plant **6**:1918–1932.

Liu, J.X., Srivastava, R., Che, P., and Howell, S.H. (2007). An endoplasmic reticulum stress response in Arabidopsis is mediated by proteolytic processing and nuclear relocation of a membrane-associated transcription factor, bZIP28. Plant Cell **19**:4111–4119.

Nakamura, Y. (2002). Towards a better understanding of the metabolic system for amylopectin biosynthesis in plants: rice endosperm as a model tissue. Plant Cell Physiol. **43**:718–725.

Nijhawan, A., Jain, M., Tyagi, A.K., and Khurana, J.P. (2008). Genomic survey and gene expression analysis of the basic leucine zipper transcription factor family in rice. Plant Physiol. **146**:333–350.

Nishi, A., Nakamura, Y., Tanaka, N., and Satoh, H. (2001). Biochemical and genetic analysis of the effects of amylose-extender mutation in rice endosperm. Plant Physiol. **127**:459–472.

Pan, T., Wang, Y., Jing, R., Wang, Y., Wei, Z., Zhang, B., Lei, C., Qi, Y., Wang, F., Bao, X., et al. (2021). Post-Golgi trafficking of rice storage proteins requires the small GTPase Rab7 activation complex MON1-CCZ1. Plant Physiol. **187**:2174–2191.

Pobre, K.F.R., Poet, G.J., and Hendershot, L.M. (2019). The endoplasmic reticulum (ER) chaperone BiP is a master regulator of ER functions: getting by with a little help from ERdj friends. J. Biol. Chem. **294**:2098–2108.

Ren, Y., Huang, Z., Jiang, H., Wang, Z., Wu, F., Xiong, Y., and Yao, J. (2021). A heat stress responsive NAC transcription factor heterodimer plays key roles in rice grain filling. J. Exp. Bot. **72**:2947–2964.

Ren, Y., Wang, Y., Liu, F., Zhou, K., Ding, Y., Zhou, F., Wang, Y., Liu, K., Gan, L., Ma, W., et al. (2014). GLUTELIN PRECURSOR ACCUMULATION3 encodes a regulator of post-Golgi vesicular traffic essential for vacuolar protein sorting in rice endosperm. Plant Cell **26**:410–425.

Ren, Y., Wang, Y., Pan, T., Wang, Y., Wang, Y., Gan, L., Wei, Z., Wang, F., Wu, M., Jing, R., et al. (2020). GPA5 encodes a Rab5a effector required for post-golgi trafficking of rice storage proteins. Plant Cell **32**:758–777.

Satoh-Cruz, M., Crofts, A.J., Takemoto-Kuno, Y., Sugino, A., Washida, H., Crofts, N., Okita, T.W., Ogawa, M., Satoh, H., and Kumamaru, T. (2010). Protein disulfide isomerase like 1-1 participates in the maturation of proglutelin within the endoplasmic reticulum in rice endosperm. Plant Cell Physiol. **51**:1581–1593.

Sun, S., Tang, X., Guo, Y., and Hu, J. (2021). Endoplasmic reticulum composition and form: proteins in and out. Curr. Opin. Cell Biol. **71**:1–6.

Takahashi, H., Kawakatsu, T., Wakasa, Y., Hayashi, S., and Takaiwa, F. (2012). A rice transmembrane bZIP transcription factor, OsbZIP39, regulates the endoplasmic reticulum stress response. Plant Cell Physiol. **53**:144–153.

Takahashi, H., Saito, Y., Kitagawa, T., Morita, S., Masumura, T., and Tanaka, K. (2005). A novel vesicle derived directly from endoplasmic

reticulum is involved in the transport of vacuolar storage proteins in rice endosperm. Plant Cell Physiol **46**:245–249.

Takemoto, Y., Coughlan, S.J., Okita, T.W., Satoh, H., Ogawa, M., and Kumamaru, T. (2002). The rice mutant esp2 greatly accumulates the glutelin precursor and deletes the protein disulfide isomerase. Plant Physiol. **128**:1212–1222.

Tian, Z., Qian, Q., Liu, Q., Yan, M., Liu, X., Yan, C., Liu, G., Gao, Z., Tang, S., Zeng, D., et al. (2009). Allelic diversities in rice starch biosynthesis lead to a diverse array of rice eating and cooking qualities. Proc. Natl. Acad. Sci. USA. **106**:21760–21765.

Umemoto, T., Aoki, N., Lin, H., Nakamura, Y., Inouchi, N., Sato, Y., Yano, M., Hirabayashi, H., and Maruyama, S. (2004). Natural variation in rice starch synthase IIa affects enzyme and starch properties. Funct. Plant Biol. **31**:671–684.

Vicente-Carbajosa, J., Moose, S.P., Parsons, R.L., and Schmidt, R.J. (1997). A maize zinc-finger protein binds the prolamin box in zein gene promoters and interacts with the basic leucine zipper transcriptional activator Opaque2. Proc. Natl. Acad. Sci. USA. **94**:7685–7690.

Wakasa, Y., Yasuda, H., Oono, Y., Kawakatsu, T., Hirose, S., Takahashi, H., Hayashi, S., Yang, L., and Takaiwa, F. (2011). Expression of ER quality control-related genes in response to changes in BiP1 levels in developing rice endosperm. Plant J. **65**:675–689.

Wang, J., Chen, Z., Zhang, Q., Meng, S., and Wei, C. (2020). The NAC transcription factors OsNAC20 and OsNAC26 regulate starch and storage protein synthesis. Plant Physiol. **184**:1775–1791.

Wang, J.C., Xu, H., Zhu, Y., Liu, Q.Q., and Cai, X.L. (2013). OsbZIP58, a basic leucine zipper transcription factor, regulates starch biosynthesis in rice endosperm. J. Exp. Bot. **64**:3453–3466.

Wang, Y., Liu, F., Ren, Y., Wang, Y., Liu, X., Long, W., Wang, D., Zhu, J., Zhu, X., Jing, R., et al. (2016). GOLGI TRANSPORT 1B regulates protein export from the endoplasmic reticulum in rice endosperm cells. Plant Cell **28**:2850–2865.

Wang, Y., Ren, Y., Liu, X., Jiang, L., Chen, L., Han, X., Jin, M., Liu, S., Liu, F., Lv, J., et al. (2010). OsRab5a regulates endomembrane organization and storage protein trafficking in rice endosperm cells. Plant J. **64**:812–824.

Wang, Y., Zhu, S., Liu, S., Jiang, L., Chen, L., Ren, Y., Han, X., Liu, F., Ji, S., Liu, X., et al. (2009). The vacuolar processing enzyme OsVPE1 is required for efficient glutelin processing in rice. Plant J. **58**:606–617.

Washida, H., Sugino, A., Doroshenk, K.A., Satoh-Cruz, M., Nagamine, A., Katsube-Tanaka, T., Ogawa, M., Kumamaru, T., Satoh, H., and Okita, T.W. (2012). RNA targeting to a specific ER sub-domain is required for efficient transport and packaging of α-globulins to the protein storage vacuole in developing rice endosperm. Plant J. **70**:471–479.

Wei, X., Jiao, G., Lin, H., Sheng, Z., Shao, G., Xie, L., Tang, S., Xu, Q., and Hu, P. (2017). GRAIN INCOMPLETE FILLING 2 regulates grain filling and starch synthesis during rice caryopsis development. J. Integr. Plant Biol. **59**:134–153.

Xiong, Y., Ren, Y., Li, W., Wu, F., Yang, W., Huang, X., and Yao, J. (2019). NF-YC12 is a key multi-functional regulator of accumulation of grain storage substances in rice. J. Exp. Bot. **70**:3765–3780.

Xu, J.J., Zhang, X.F., and Xue, H.W. (2016). Rice aleurone layer specific OsNF-YB1 regulates grain filling and endosperm development by interacting with an ERF transcription factor. J. Exp. Bot. **67**:6399–6411.

Yamagata, H., Sugimoto, T., Tanaka, K., and Kasai, Z. (1982). Biosynthesis of storage proteins in developing rice grains. Plant Physiol. **70**:1094–1100.

Yang, W., Xu, P., Zhang, J., Zhang, S., Li, Z., Yang, K., Chang, X., and Li, Y. (2022). OsbZIP60-mediated unfolded protein response regulates grain chalkiness in rice. Journal of Genetics and Genomics **49**:414–426.

Yang, Y., Guo, M., Li, R., Shen, L., Wang, W., Liu, M., Zhu, Q., Hu, Z., He, Q., Xue, Y., et al. (2015). Identification of quantitative trait loci responsible for rice grain protein content using chromosome segment substitution lines and fine mapping of qPC-1 in rice (*Oryza sativa* L.). Mol. Breeding **35**:130.

Yasuda, H., Hirose, S., Kawakatsu, T., Wakasa, Y., and Takaiwa, F. (2009). Overexpression of BiP has inhibitory effects on the accumulation of grain storage proteins in endosperm cells of rice. Plant Cell Physiol. **50**:1532–1543.

Zhang, C., Zhu, J., Chen, S., Fan, X., Li, Q., Lu, Y., Wang, M., Yu, H., Yi, C., Tang, S., et al. (2019a). Wx-lv, the ancestral allele of rice waxy gene. Mol. Plant **12**:1157–1166.

Zhang, Z., Dong, J., Ji, C., Wu, Y., and Messing, J. (2019b). NAC-type transcription factors regulate accumulation of starch and protein in maize grains. Proc. Natl. Acad. Sci. USA. **116**:11223–11228.

Yang, T., Guo, L., Ji, C., Wang, H., Wang, J., Zheng, X., Xiao, Q., and Wu, Y. (2021). The B3 domain-containing transcription factor ZmABI19 coordinates expression of key factors required for maize grain development and grain filling. Plant Cell **33**:104–128.

Zhang, Z., Zheng, X., Yang, J., Messing, J., and Wu, Y. (2016). Maize endosperm-specific transcription factors O2 and PBF network the regulation of protein and starch synthesis. Proc. Natl. Acad. Sci. USA. **113**:10842–10847.

Zhu, J., Ren, Y., Wang, Y., Liu, F., Teng, X., Zhang, Y., Duan, E., Wu, M., Zhong, M., Hao, Y., et al. (2019). OsNHX5-mediated pH homeostasis is required for post-Golgi trafficking of grain storage proteins in rice endosperm cells. BMC Plant Biol. **19**:295.

Zhu, J., Ren, Y., Zhang, Y., et al. (2021). Subunit E isoform 1 of vacuolar H+-ATPase OsVHA enables post-Golgi trafficking of rice seed storage proteins. Plant Physiol **187**:2192–2208.

Plant Communications, Volume *3*

Supplemental information

OPAQUE3, encoding a transmembrane bZIP transcription factor, regulates endosperm storage protein and starch biosynthesis in rice

Ruijie Cao, Shaolu Zhao, Guiai Jiao, Yingqing Duan, Liuyang Ma, Nannan Dong, Feifei Lu, Mingdong Zhu, Gaoneng Shao, Shikai Hu, Zhonghua Sheng, Jian Zhang, Shaoqing Tang, Xiangjin Wei, and Peisong Hu

Supplemental Information:

OPAQUE3, encoding a transmembrane bZIP transcription factor, regulates endosperm storage protein and starch biosynthesis in rice

Ruijie Cao[1,3], Shaolu Zhao[1,2,3], Guiai Jiao[1], Yingqing Duan[1], Liuyang Ma[1], Nannan Dong[1], Feifei Lu[1], Mingdong Zhu[1], Gaoneng Shao[1], Shikai Hu[1], Zhonghua Sheng[1], Jian Zhang[1], Shaoqing Tang[1], Xiangjin Wei[1,*], Peisong Hu[1,*]

[1] State Key Laboratory of Rice Biology, China National Center for Rice Improvement, China National Rice Research Institute, Hangzhou, 310006, China

[2] Institute of Agricultural Science in Jiangsu Coastal Areas, Yancheng, 224002, China

[3] These authors contributed equally to this work.

* Correspondence: Xiangjin Wei (weixiangjin@caas.cn), Peisong Hu (peisonghu@126.com, hupeisong@caas.cn)

Supplemental Figures 1-14

Supplemental Tables 1

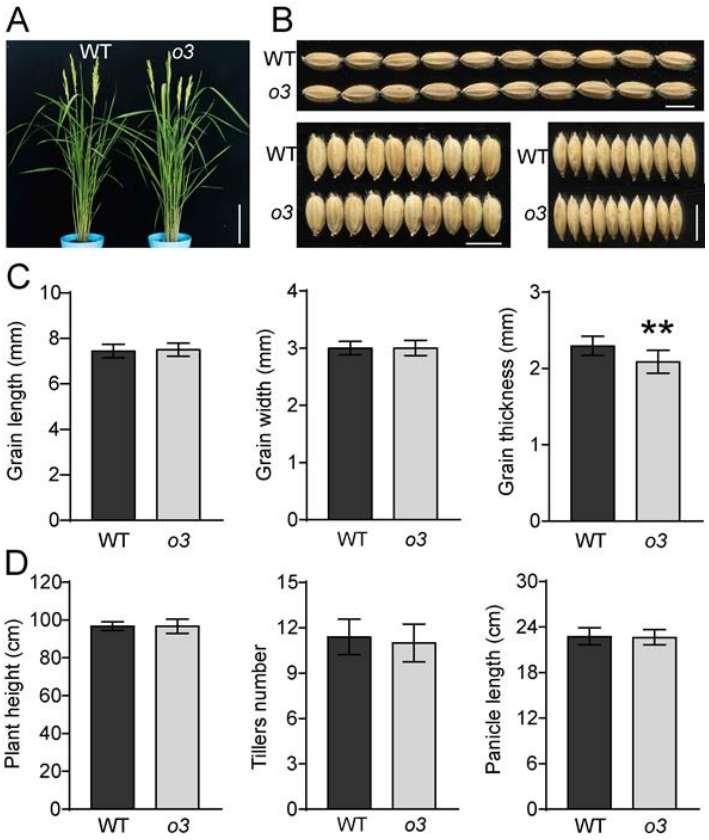

Figure S1. Characteristics of wild type (WT) and *o3* mutant.

(A) The plant phenotype of WT and *o3* after heading.

(B, C) The morphology **(B)** and Statistics **(C)** of grain length, grain width and grain thickness of WT and *o3* (n=200). Scale bars, 20 cm in **(A)**; 6mm in **(B)**.

(D) Plant height, tiller number and panicle length of WT and *o3*. Values are means ±*SD* from three biological replicates, not less than 10 plants in each replication. The asterisks indicate statistical significance compared with the wild type, as determined by Student's *t*-test (**, $P < 0.01$).

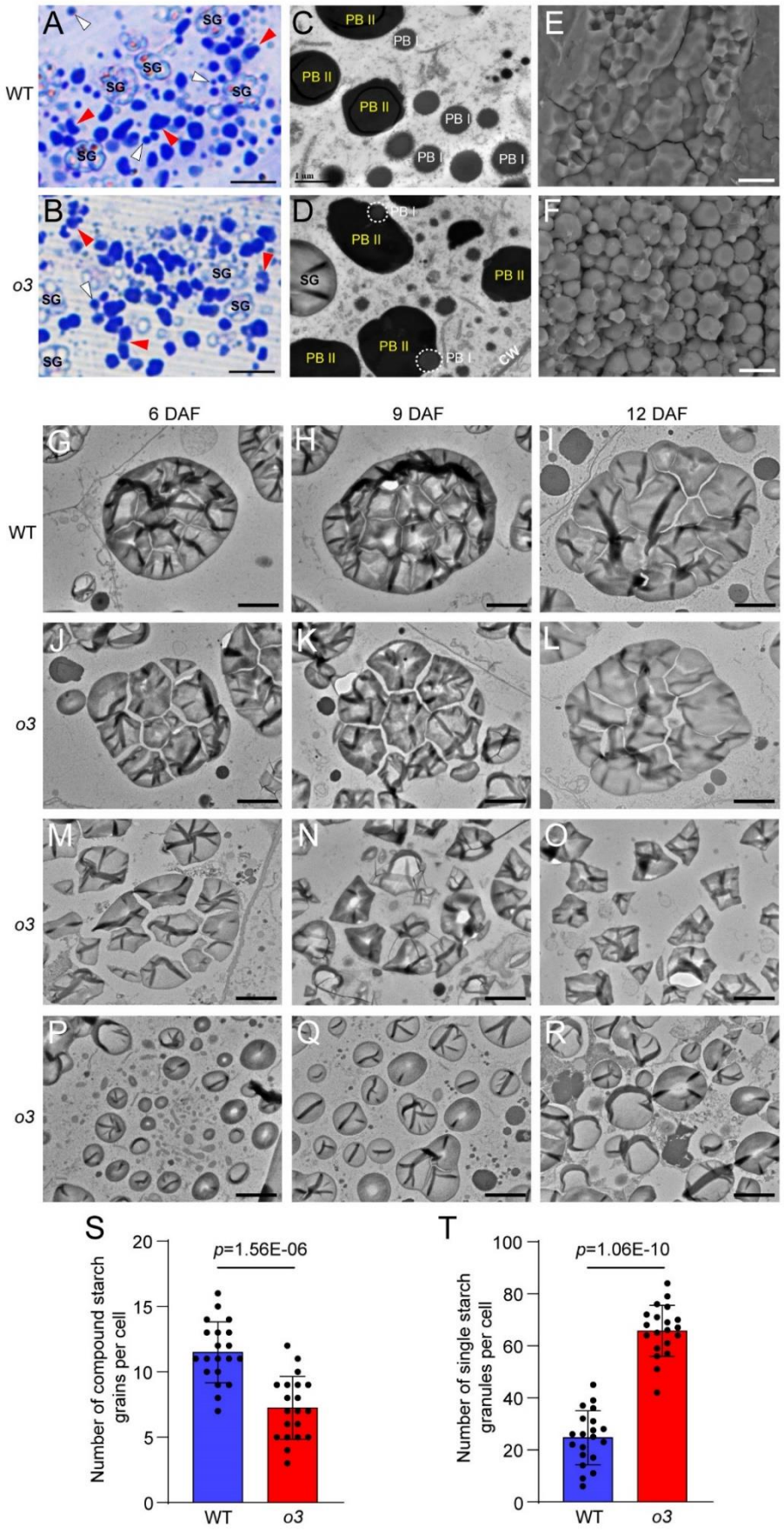

Figure S2. The morphology of protein body and starch granule in developing endosperm cells of wild type and *o3*.

(A, B) Semi-thin sections stained with Coomassie blue showing the morphology of PB I and PB II of WT and *o3* endosperm at 12 DAF. White arrowhead denotes PB I, red arrowhead denotes PB II; SG, starch granule. Scale bars, 20μm.

(C, D) Transmission electron microscopy showing the structure of PBI and PBII of WT and *o3* endosperm, White dotted line indicates the abnormal infusion of PBI and PBII. CW, cell wall. Scale bars, 1μm.

(E, F) Scanning electron microscopy images of transverse sections of mature grains of WT and *o3*. Scale bars, 10μm.

(G-I) Transmission electron microscopy (TEM) showed the well-developed amyloplast in WT endosperm cells at 6 DAF (**G**), 9 DAF (**H**), and 12 DAF (**I**). Scale bars, 2 μm.

(J-L) Few well-developed amyloplast were observed in *o3* endosperm cells at 6 DAF (**J**), 9 DAF (**K**) and 12 DAF (**L**). Scale bars, 2 μm.

(M-O) The amyloplasts were gradually disintegrated in *o3* endosperm cells from 6 DAF (**M**) to 9 DAF (**N**) and 12 DAF (**O**). Scale bars, 2 μm.

(P-R) Single and dispersive starch granules in *o3* endosperm cells at 6 DAF (**P**), 9 DAF (**Q**), and 12 DAF (**R**). Scale bars, 2 μm.

(S, T) Statistics of the number of starch compound grains and single granules in central endosperm cells of WT and *o3* at 9 DAF. Data are means ± SD from at least three biological replicates. Statistically significant differences were determined using Student's *t*-test. *P*-values are shown when statistically significant.

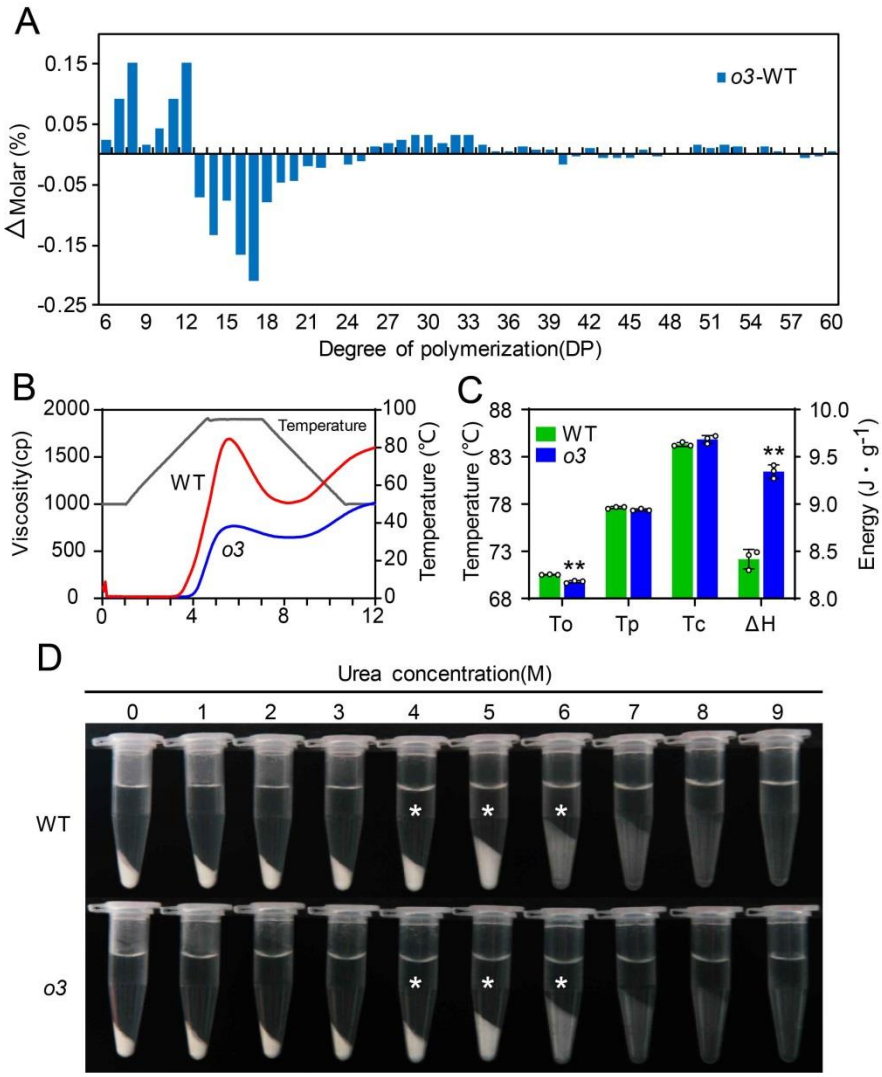

Figure S3. Starch physicochemical characteristics in the *o3* mutant.

(A) Differences in the amylopectin chain length distributions between the WT and *o3*.

(B) Pasting properties analyzing with a rapid visco analyzer (RVA) of endosperm starch of WT (red line) and *o3* (blue line). The viscosity value at each temperature is the average of three replicates. The gray line indicates the temperature changes during the measurements.

(C) Gelatinization temperature of endosperm starch. To, Tp, and Tc represent the onset, peak, and conclusion gelatinization temperatures, respectively. All data are presented as means ±SD from three replicates. Statistically significant differences were determined using Student's *t*-test (**, $P < 0.01$).

(**D**) Gelatinization characteristics of starch from *o3* mutant seeds. Starch powder was mixed with different concentrations (1~9 M) of urea solution. The most significant difference was observed for 4~6 M urea (indicated by *).

A

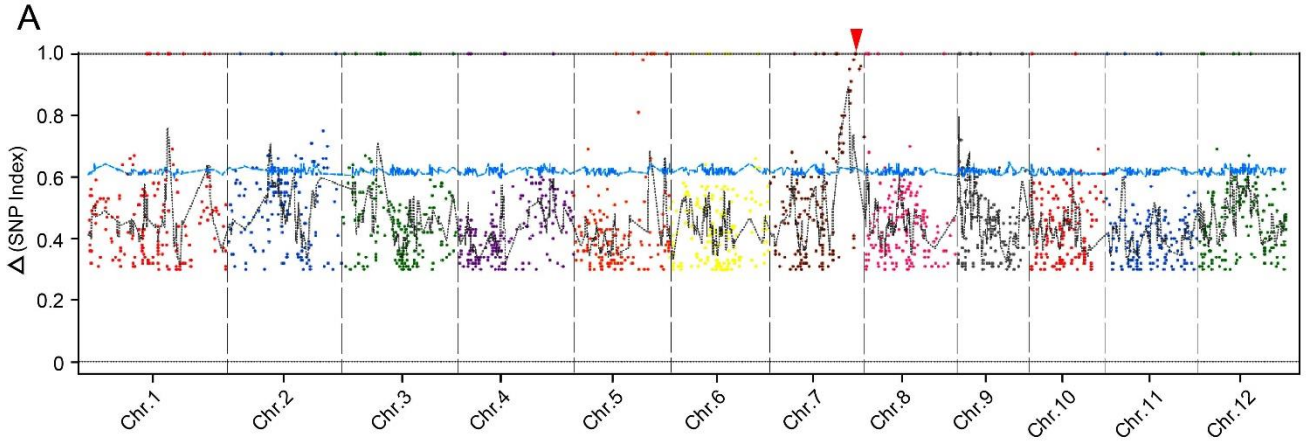

B

SNP	Position	Genotype	Δ(SNP-index)	Variant	Gene	Description
SNP1	26610760	C to T	1	synonymous SNV	LOC_Os07g44560	AMP-binding domain containing protein
SNP2	26810333	T to C	1	nonsynonymous SNV	LOC_Os07g44950	bZIP transcription factor
SNP3	26108114	C to T	0.98	intronic	LOC_Os07g43610	hypothetical protein
SNP4	28371212	C to T	0.96	upstream	LOC_Os07g47460	expressed protein
SNP5	24796636	C to T	0.95	intronic	LOC_Os07g41380	retrotransposon protein
SNP6	27900815	C to T	0.95	intronic	LOC_Os07g46680	expressed protein
SNP7	25293558	C to T	0.91	splicing	LOC_Os07g42260	OsPAA2
SNP8	24593986	T to C	0.88	intronic	LOC_Os07g41090	HDA713
SNP9	25101693	C to T	0.88	intronic	LOC_Os07g41900	expressed protein
SNP10	24969228	T to A	0.84	upstream	LOC_Os07g41660	expressed protein
SNP11	20252223	T to C	0.81	intergenic	LOC_Os05g34210	expressed protein
SNP12	23272328	G to A	0.8	upstream	LOC_Os07g38780	transposon protein
SNP13	22518789	C to T	0.8	downstream	LOC_Os07g37580	diacylglycerol kinase

Figure S4. Mut-map cloning of *O3*.

(A) Distribution of progeny Δ(SNP-index) on chromosomes of the whole genome generated using Mut-map method. The black curves represent SNP-index plot regression lines; red arrowhead indicates the SNP located on candidate gene.

(B) The annotation of 13 candidate SNPs on chromosome 7 with SNP-index more than 0.8. The candidate SNP was shown in red format.

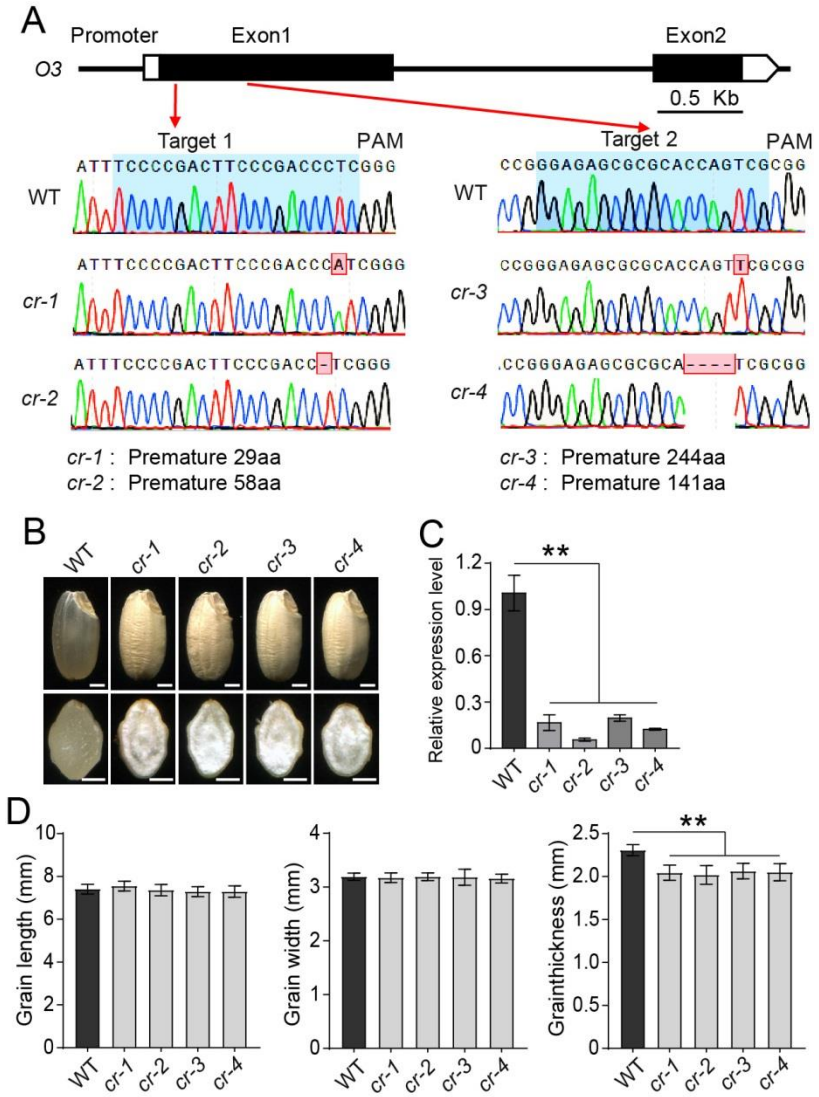

Figure S5. Analysis of CRISPR/Cas9 mediated editing lines of *O3*.

(A) Gene structure of *O3* and sequencing of CRISPR/Cas9 target region in WT and T_0 plants. Scale bars, 0.5 kb.

(B) Appearance and transverse sections of mature seeds of wild type and *O3* knock out plants (*cr-1*~*cr-4*). Scale bars, 1mm.

(C) Relative expression level of *O3* in transgenic knock out plants (*cr-1*~*cr-4*).

(D) The grain length, grain width and grain thickness of brown rice of wild type and *O3* knock out plants (*cr-1*~*cr-4*).

Data in **(C-D)** are shown as mean ± *SD* from three biological replicates. Asterisks indicate statistical significance as determined by Student's *t*-test (**$P < 0.01$).

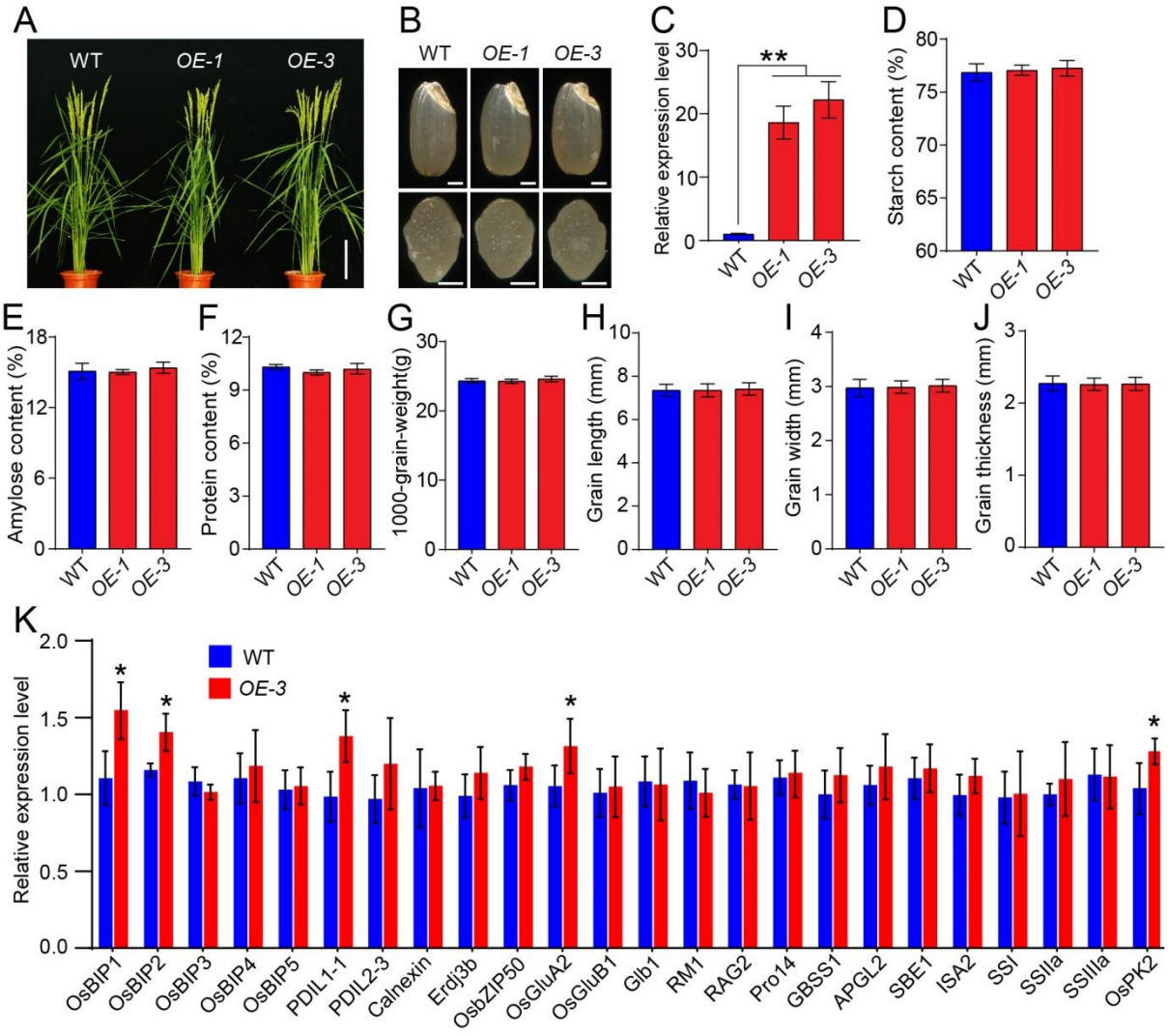

Figure S6. Analysis of overexpression lines of *O3* in WT background.

(A) The plant phenotype of WT and transgenic overexpression plants in WT background (*OE-1* and *OE-3*) after heading. Scale bar, 20 cm.

(B) Appearance and transverse sections of mature grains of WT, *OE-1* and *OE-3* plants. Scale bars, 1mm.

(C) Relative expression level of *O3* in *OE-1* and *OE-3*.

(D-G) The total starch **(D)**, amylose **(E)**, and total protein **(F)** content in endosperm, and 1000-grain-weight **(G)** of WT, *OE-1* and *OE-3*.

(H-J) The grain length **(H)**, grain width **(I)** and grain thickness **(J)** of brown rice of WT, *OE-1* and *OE-3*.

(K) RT-qPCR analysis of genes related to ER stress, and genes related to starch and protein biosynthesis in WT and *O3 OE* lines.

Data in **(C-K)** are shown as mean ± *SD* from three biological replicates, respectively. Asterisks indicate statistical significance as determined by a Student's *t*-test (**P* < 0.05, ***P* < 0.01).

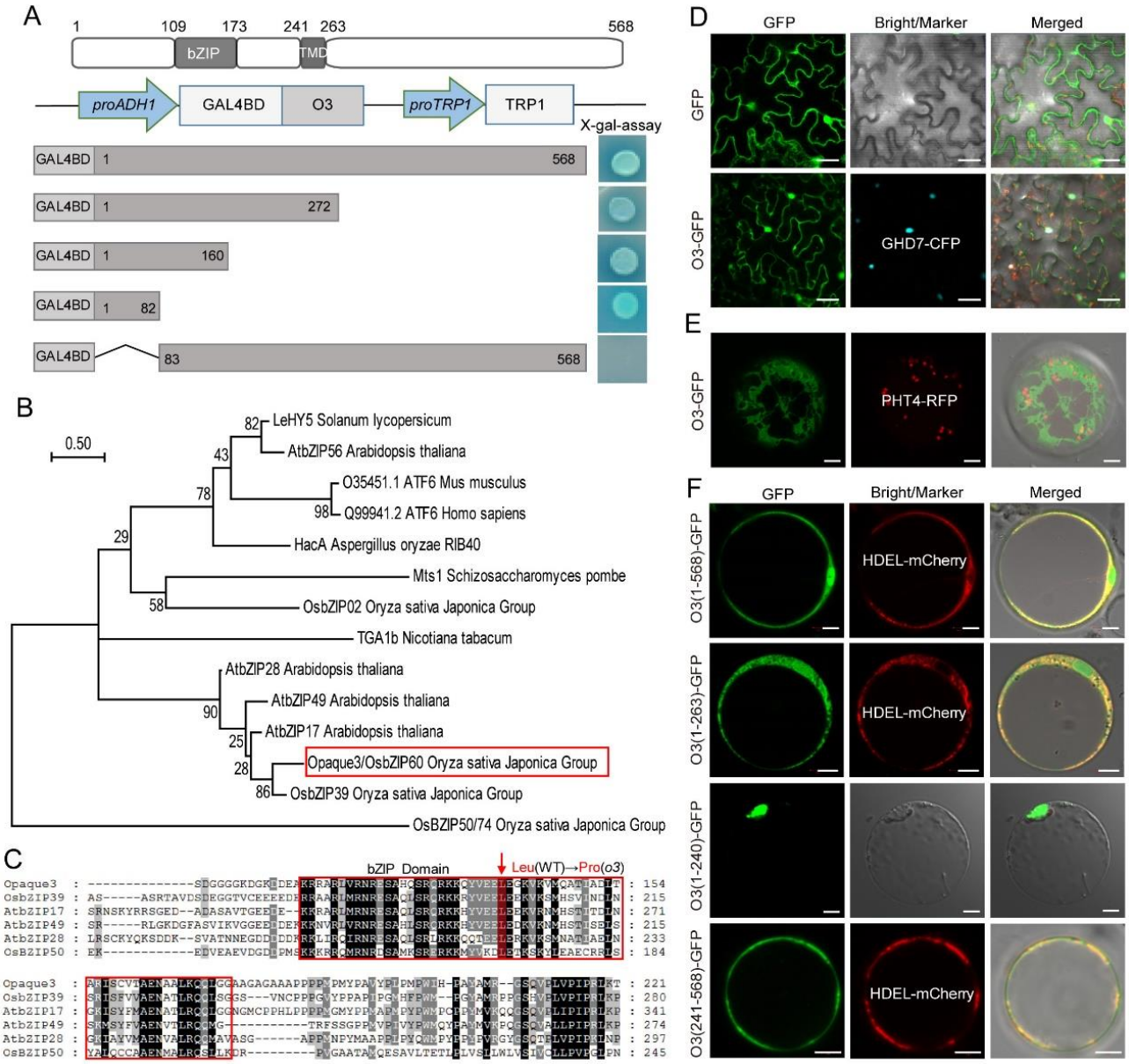

Figure S7. Molecular biological characteristics of O3

(A) Transactivation assay of different truncated form of O3. bZIP, TMD represented the basic zipper and transmembrane domain, respectively. Fusion proteins of the GAL4 DNA-binding domain and different portions of O3 were checked for their transactivation activity in yeast.

(B) Phylogenetic analysis of O3. The neighbor-joining tree was generated with MEGA7. Red box denotes the O3 in rice.

(C) Amino acid sequence alignment between part of O3 and other homologous proteins. It was generated with ClustalX2. White alphabet with black, grey background, and black alphabet with light grey background stands 100%, 80%, and 60% identity, respectively. Red box denotes the bZIP domain of O3 and other homologous proteins. Red arrow indicates the most conserved amino acid (lysine) of these homologous genes.

(D) Subcellular localization of O3-GFP in *N.benthamiana* leaves. O3-GFP is co-localized with GHD7-CFP in nucleus. Scale bars, 20μm.

(E) Subcellular localization of Full-length O3-GFP showing it is not co-localized with PHT4-RFP signal in Golgi. Scale bars, 5μm.

(F) Subcellular localization of different truncated forms of O3 in rice protoplast. $O3^{1\text{-}240aa}$–GFP is only localized in nucleus. $O3^{1\text{-}263aa}$-GFP and $O3^{1\text{-}568aa}$-GFP are co-localized in nucleus and ER. $O3^{241\text{-}568aa}$-GFP is only co-localized with HDEL-mCherry signal in ER. Scale bars, 5μm.

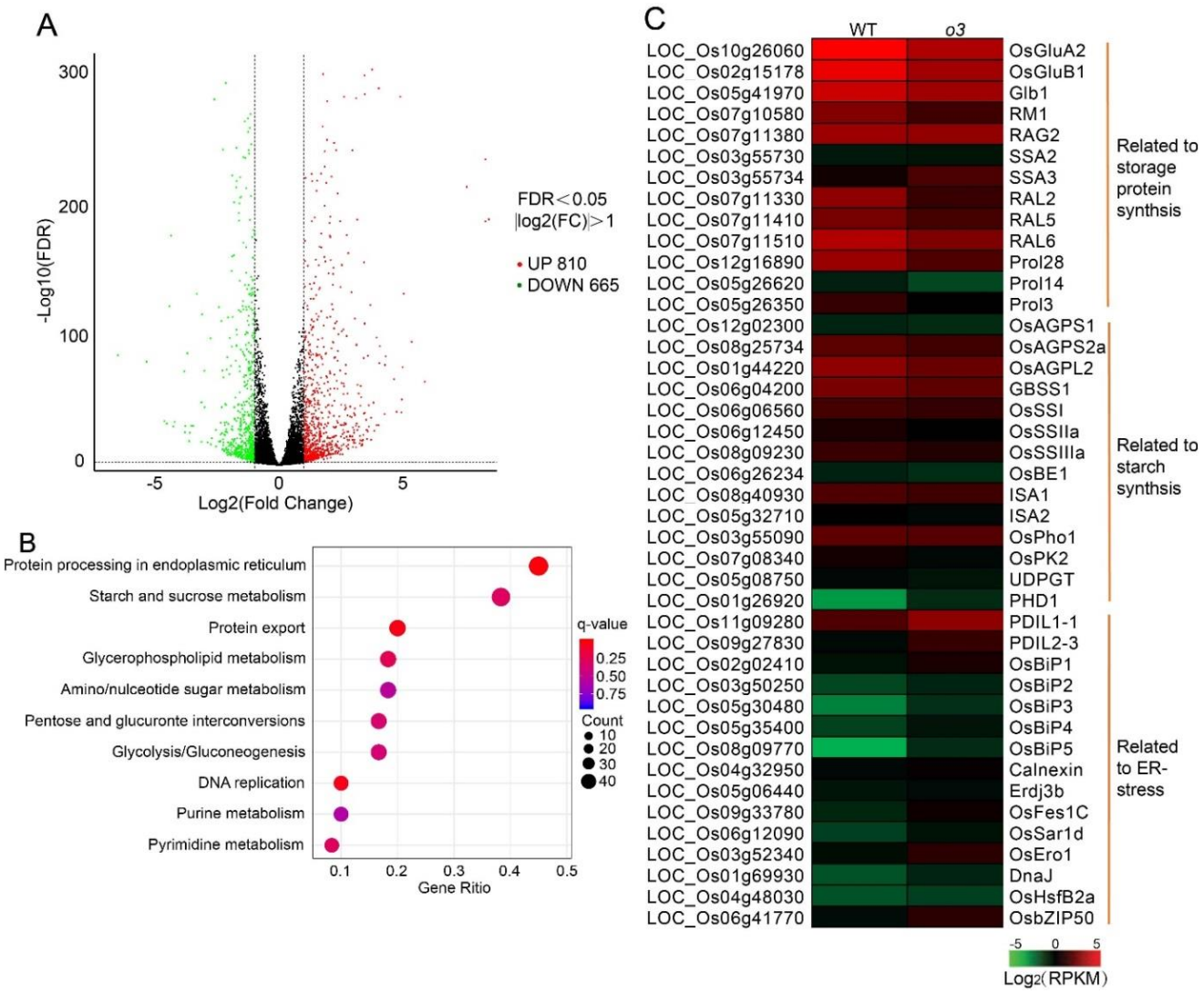

Figure S8. RNA-seq analysis of wild type and *o3* using grains at 12 DAF.

(A) Genes up- or down-regulated in RNA-seq data. A volcano plot of differential transcription levels between WT and *o3* Green dots indicate reduced transcription level; red dots indicated increased transcription level; blue dots indicate no difference between WT and *o3*.

(B) GO enrichment terms for the 159 DEGs (differentially expressed genes) shared among the three groups.

(C) Heat map of the differentially regulated genes in WT and *o3* from RNA-seq. Genes related to ER stress were up-regulated while genes related to storage protein and starch synthesis were down-regulated. Data are shown as means ±SD from three individual replicates.

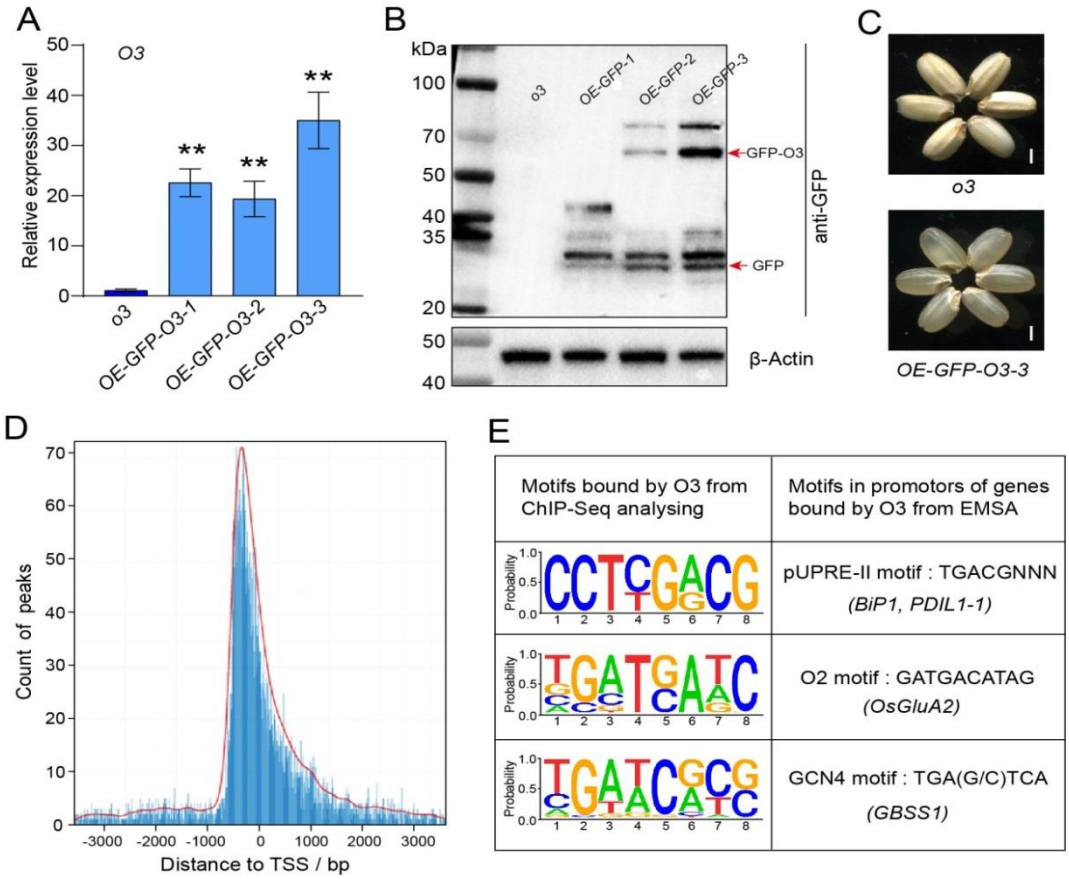

Figure S9. ChIP-seq analysis in grains at 9 DAF from *GFP-O3* overexpression lines.

(A) Relative expression level of *O3* in grains of *o3* mutant and *OE-GFP-O3* lines in *o3* background.

(B) The western blot detection of the GFP-O3 fusion protein level in 9-DAF grains of *o3* mutant and *OE-GFP-O3* overexpression lines using GFP antibodies.

(C) The appearance of mature grains of *o3* mutant and *OE-GFP-O3-3* line in *o3* background. *OE-GFP-O3-3* line was used for ChIP-seq. Scale bars, 1mm.

(D) Distribution of O3 binding peaks corresponding to the -3000bp to +3000bp region flanking the transcriptional start site (TSS).

(E) Three high-frequency motifs contained in the O3 binding peaks from ChIP-seq.

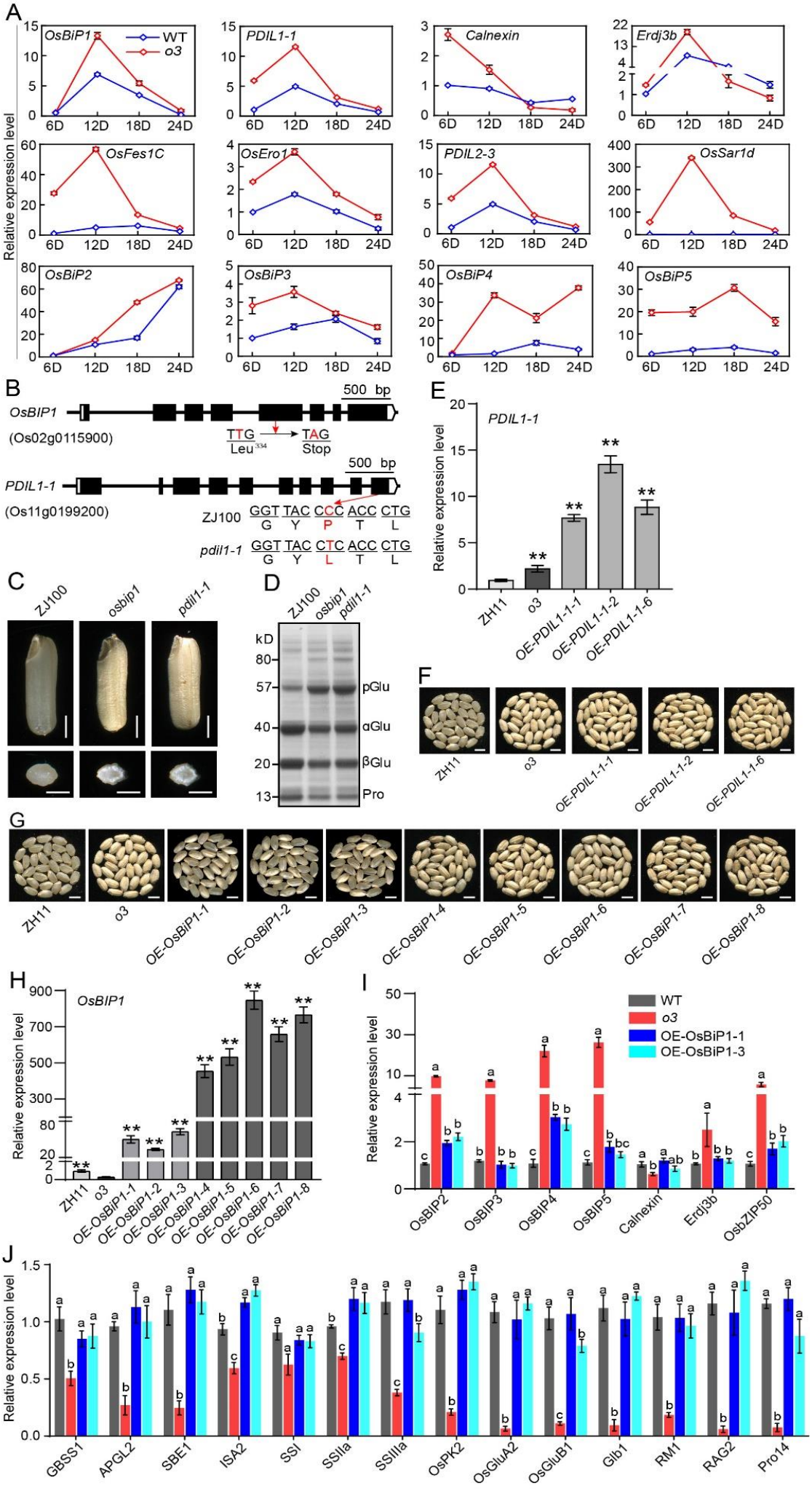
A
OsBiP1
WT
o3
PDIL1-1
Calnexin
Erdj3b
OsFes1C
OsEro1
PDIL2-3
OsSar1d
OsBiP2
OsBiP3
OsBiP4
OsBiP5
Relative expression level
6D 12D 18D 24D
B
OsBIP1
(Os02g0115900)
500 bp
TTG Leu334 TAG Stop
PDIL1-1
(Os11g0199200)
ZJ100 GGT TAC CCC ACC CTG
G Y P T L
pdil1-1 GGT TAC CTC ACC CTG
G Y L T L
C
ZJ100
osbip1
pdil1-1
D
kD
80
57
40
20
13
pGlu
αGlu
βGlu
Pro
E
PDIL1-1
Relative expression level
ZH11
o3
OE-PDIL1-1-1
OE-PDIL1-1-2
OE-PDIL1-1-6
F
G
ZH11
o3
OE-OsBiP1-1
OE-OsBiP1-2
OE-OsBiP1-3
OE-OsBiP1-4
OE-OsBiP1-5
OE-OsBiP1-6
OE-OsBiP1-7
OE-OsBiP1-8
H
OsBIP1
Relative expression level
I
WT
o3
OE-OsBiP1-1
OE-OsBiP1-3
Relative expression level
OsBIP2
OsBIP3
OsBIP4
OsBIP5
Calnexin
Erdj3b
OsbZIP50
J
Relative expression level
GBSS1
APGL2
SBE1
ISA2
SSI
SSIIa
SSIIIa
OsPK2
OsGluA2
OsGluB1
Glb1
RM1
RAG2
Pro14

Figure S10. The grains phenotype of *osbip1* and *pdil1-1* mutant in ZJ100 background

(A) Relative expression level of genes (*OsBIP1~OsBIP5, PDIL1-1, PDIL2-3, Calnexin, Erdj3b, OsFes1C, OsEro1*, *OsSarld*) related to ER stress in developing endosperm at 6, 12, 18, 24 days after fertilization.

(B) The mutation type of *OsBIP1* and *PDIL1-1* in ZhongJian100 (ZJ100) background.

(C) Grains appearance of *osbip1* and *pdil1-1* in ZJ100 background. Scale bars, 2mm.

(D) SDS-PAGE profiles of total dry-seed storage proteins of ZJ100, *osbip1*, and *pdil1-1* mutants. pGlu, 57-kDa proglutelins; αGlu, 40-kDa glutelin acidic subunits; βGlu, 20-kDa glutelin basic subunits; Pro, prolamins.

(E) RT-qPCR analysis of *PDIL1-1* transcription level in transgenic over-expression lines in the *o3* mutant background (*OE-PDIL1-1*).

(F) Grains appearance of *OE-PDIL1-1* lines. Scale bars, 5mm.

(G) Grains appearance of *OsBIP1* over-expression lines in the *o3* mutant background (*OE-OsBIP1*). *OE-OsBIP1-1~3* could partly restore the transparent endosperm phenotype, but *OE-OsBIP1-4~8* failed to rescue the *o3* phenotype. Scale bars, 5mm.

(H-J) RT-qPCR analysis of *OsBIP1* **(H)**, genes related to ER stress **(I)**, and genes related to starch and protein biosynthesis **(J)** in *OE-PDIL1-1* lines.

Data in **(A, E, H-J)** are shown as means ±SD from three individual replicates. Statistically significant differences were determined using Student's *t*-test (indicated with different lowercase letters ($P < 0.05$), or * $P < 0.05$; **, $P < 0.01$).

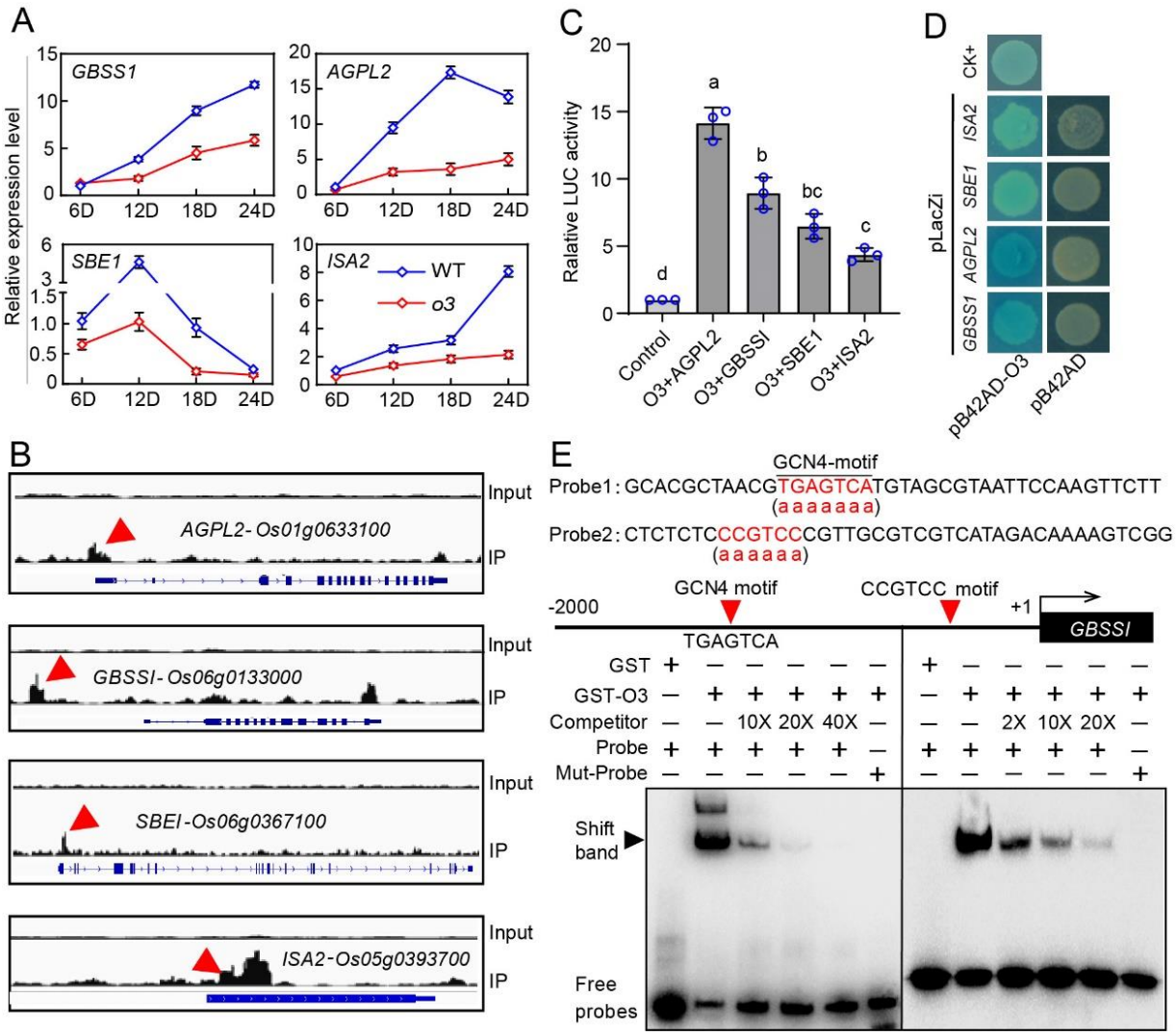

Figure S11. O3 directly activate the transcription of genes related to starch synthesis.

(A) RT-qPCR analysis of *GBSS1*, *AGPL2*, *SBE1*, *and ISA2* transcription level in developing endosperm at 6, 12, 18, 24 days after fertilization. Data are shown as means ±SD (n=3).

(B) Chip-seq results showing the distributions of O3 binding sites for *GBSS1*, *AGPL2*, *SBE1*, and *ISA2* loci, as shown in Integrative Genomics Viewer. Red arrowhead indicates significant peaks calculated by MACS2, and the positions of peaks were shown in Attachment data II. Input sample was used as a negative control.

(C) Luciferase transient transactivation assay in rice protoplasts. O3 significantly activated the transcription of *GBSS1, AGPL2, SBE1* and *ISA2.* Data are shown as means ±SD (n=3), significant difference was labeled with different letters according to Student's *t*-test.

(D) Yeast-one-hybrid assay showing the binding of O3 to the promotor of *GBSS1*, *AGPL2*, *SBE1*, *ISA2*.

(E) EMSA showed that O3 could bind to the probes of *GBSS1* with GCN4-motif (probe1, left) and CCGTCC-motif (probe2, right), the mutated motif in mut-probes was showed in bracket.

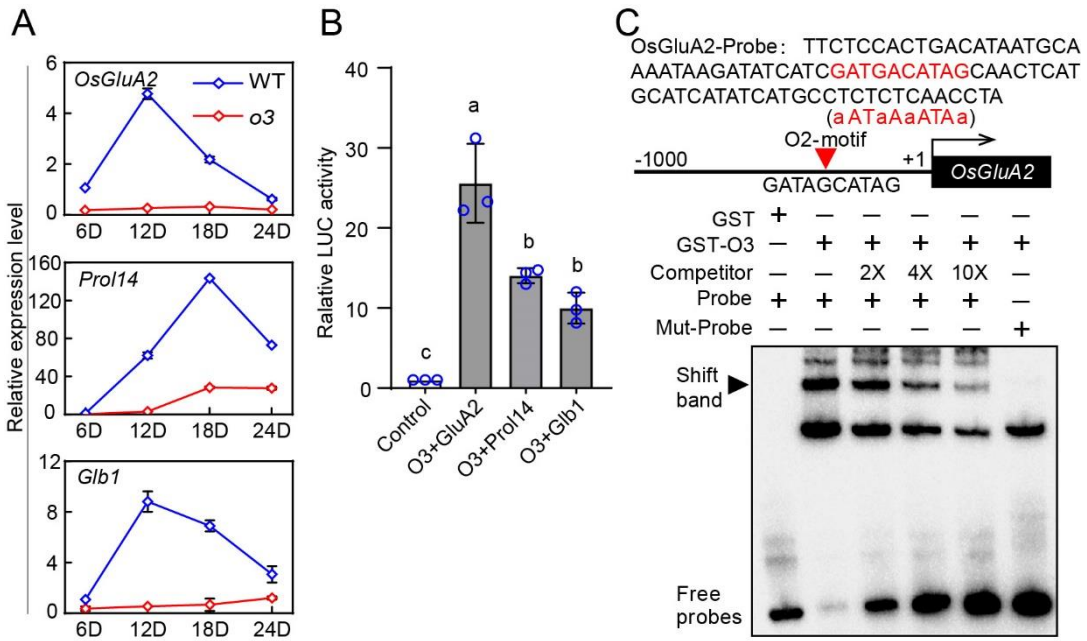

Figure S12. O3 directly activate the expression of genes related to protein synthesis.

(A) RT-qPCR analysis of *OsGluA2*, *Prol14*, and *Glb1* transcription level in developing endosperm at 6, 12, 18, 24 from 6~24 days after fertilization. Data are shown as means ±SD (n=3).

(B) Luciferase transient transactivation assay in rice protoplasts. O3 significantly activated the transcription of *OsGluA2*, *Prol14*, and *Glb1*. Data are shown as means ±SD (n=3), significant difference was labeled with different letters according to Student's *t*-test (n=3).

(C) EMSA showed that O3 could bind to the probes of *GBSS1* with O2-motif; the mutated motif in mut-probes was showed in bracket.

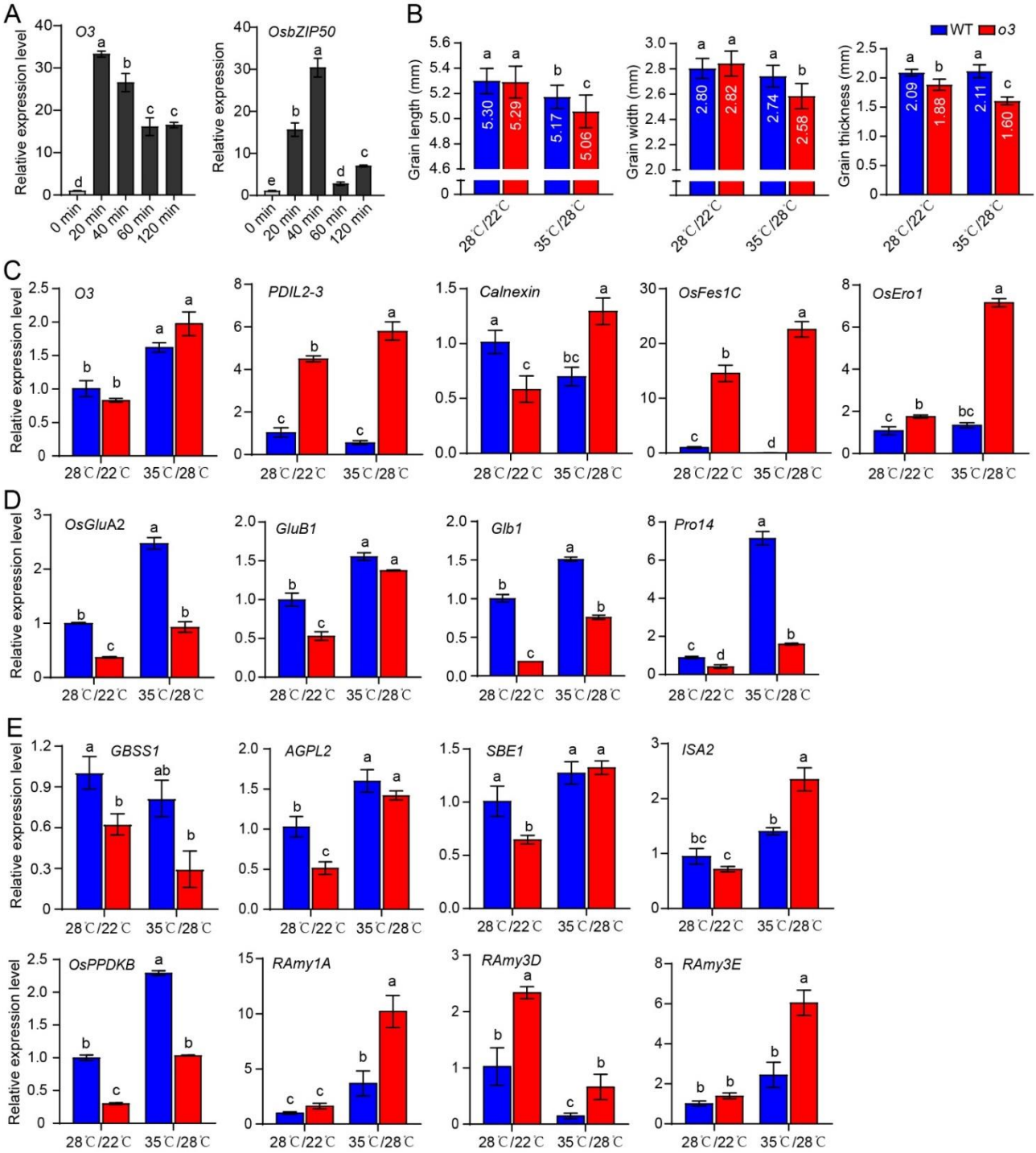

Figure S13. *o3* undergo more serious ER stress under high-temperature conditions.

(A) Relative expression level of *O3 and OsbZIP50* in 2-week-old seedlings under heat stress treatment (42°C).

(B) Grain length, grain width and grain thickness of WT and *o3* under high-temperature treatment (35°C, 12h light /28°C, 12h, Dark) and normal-temperature treatment (28°C, 12h light /22°C, 12h, Dark).

(C-E) Relative expression levels of genes related to ER stress **(C),** protein synthesis **(D**) and starch synthesis **(E)**.

Values are means ± SD from three biological replicates. Significant difference was labeled with different letters according to Student's *t*-test.

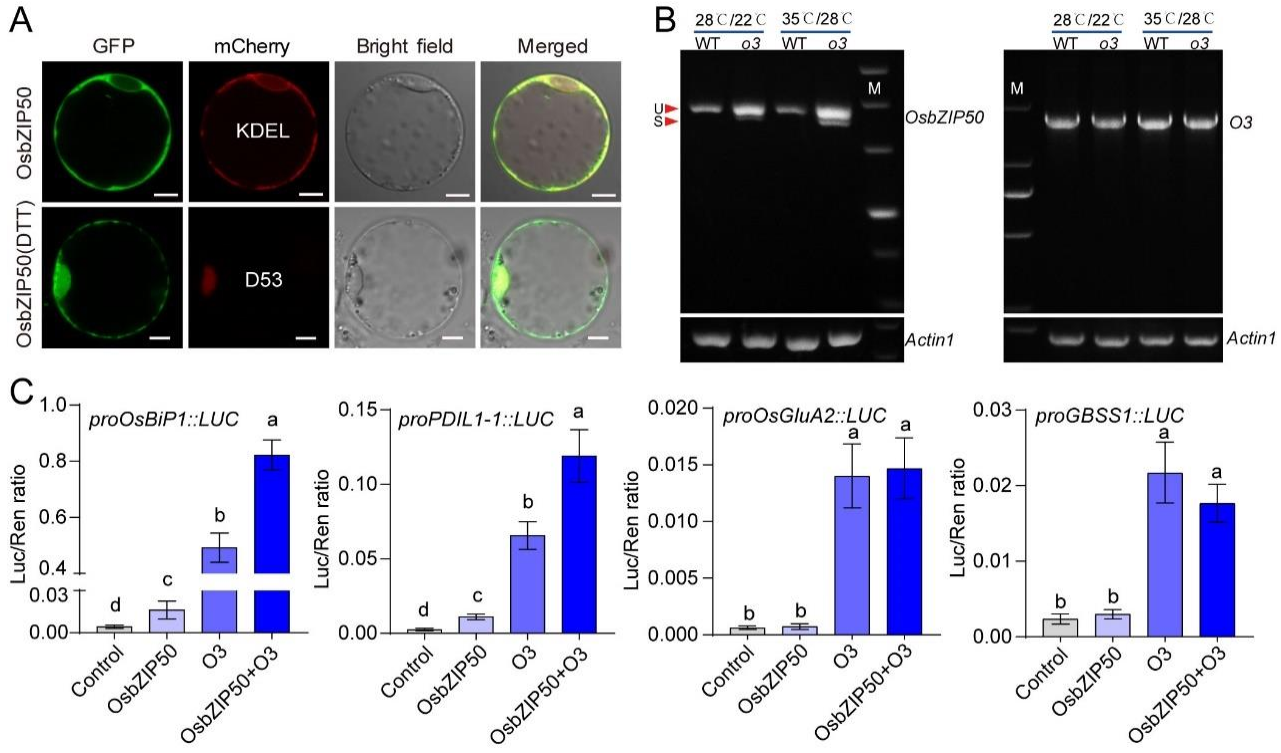

Figure S14. OsbZIP50 can assist O3 in response to the ER stress.

(A) Subcellular localization of OsbZIP50 in rice protoplast. OsbZIP50-GFP was localized in cytoplasm and co-localized with HDEL-mCherry signal in ER. OsbZIP50-GFP was co-localized with DWARF53(D53)-mCherry signal in nucleus after 2 hours Dithiothreitol (DTT) treatment. Scale bars, 5 μm.

(B) The splicing forms of *OsbZIP50* and *O3* mRNA were detected in the wild type and *o3* mutant. The semi-quantitative RT-PCR analysis of *OsbZIP50* and *O3* transcripts in endosperm cells of WT and *o3* under high- and normal-temperature conditions. U, un-spliced form; S, spliced form.

(C) Transactivation assay of OsbZIP50 and O3 for *OsBIP1*, *PDIL1-1*, *OsGluA2*, and *GBSS1* in rice protoplasts. Luciferase reporter assay shows that OsbZIP50 can enhance the transient transactivation of *OsBIP1* and *PDIL1-1* together with O3. Values are means ± SD from three biological replicates. Significant difference was labeled with different letters according to Student's *t*-test.

Table S1. Primers used in this study

Mapping	RM22097-F	AAGAAATTCAAAACACATGA
	RM22097-R	AAAACATCTACTTTGATCCA
	RM22166-F	TCCTTGTGAAATCTGGTCCC
	RM22166-R	GTAGCCTAGCATGGTGCATG
Sequencing	03-F	CGCACCTTCGCTCTCTTTTCC
	03-R	ACCTGCGAGCCACGCATTGC
	OsbZIP39-F	ATGGCGGAGCCGGCCCTGCTG
	OsbZIP39-R	GCACTTGGCCGCGTCCGAGCT
	OsbZIP50-F	GGCAACCCACCGCGAGAGAC
	OsbZIP50-R	CTCTCCCTCGATTTCATGGC
Binary vector construction	1300-O3-KpnI-F	AATTCGAGCTCGGTACCAGGCGCAATTGCCTTATGAAG
	1300-O3-Sal1-R	GCATGCCTGCAGGTCGACTTGGAACGCGAAAACCTCAG
	RHV-O3-Sac1-F	GGATCCCCGGGTGAGCTCATGGCGGAGCCGGACCTACTC
	RHV-O3-HindIII-R	GCCGCACTAGTAAGCTTCAAGTGAGGGCTATGGCTTTTG
	GUS-O3-EcoRI-F	CCATGATTACGAATTCAGGAGTCCTGGTCATCTTCT
	GUS-O3-NcoI-R	CTCAGATCTACCATGGCCAGATCGTCGAGATCGAAA
Crispr Cas9	Crispr-O3-Target1-F	ggcACCCCGACTTCCCGACCCTCG
	Crispr-O3-Target1-R	aaacCGAGGGTCGGGAAGTCGGGG
	Crispr-O3-Target2-F	ggcAGGGAGAGCGCGCACCAGTCG
	Crispr-O3-Target2-R	aaacCGACTGGTGCGCGCTCTCCC
	Crispr-OsbZIP39-F	gccGGGCTCGAGTTCGACCTGCC
	Crispr-OsbZIP39-R	aaacGGCAGGTCGAACTCGAGCC
	Crispr-OsbZIP50-F	gttGAGTGAGGCGGGGGGAAGCA
	Crispr-OsbZIP50-R	aaacTGCTTCCCCCCGCCTCACT
Subcellular localization	PAN580-O3-XbaI-F	AGTCCGGAGCTAGCTCTAGAATGGCGGAGCCGGACCTACT
	PAN580-O3-BamHI-R	CCCTTGCTCACCATGGATCCCAAGTGAGGGCTATGGCTTT
	PAN580-O3(1-240)-BamHI-R	CCCTTGCTCACCATGGATCCCTTCTTGGTCTTCCGGGCCTT
	PAN580-O3(1-263)-BamHI-R	GTCCGGAGCTAGCTCTAGAAATCGGATGTATGGTGCAGCG
	PAN580-OsbZIP50-XbaI-F	AGTCCGGAGCTAGCTCTAGAATGACATGGCACATTCAAGC
	PAN580-OsbZIP50-BamHI-R	CCCTTGCTCACCATGGATCCGCAAGCAGCTGCTGCTAAAC
	pYBA1132-O3-Xba1-F	GGTGGCGGCCGCTCTAGAATGGCGGAGCCGGACCTACT
	pYBA1132-O3-Kpn1-R	CTTGCTCACCATGGTACCCAAGTGAGGGCTATGGCTTT
	mCherry-D53-F	AGCCCAGATCACTAGTATGCCCACTCCGGTGGCCGCC
	mCherry-D53-R	TGCTCACCATGGATCCACAATCTAGAATTATTCTTGGC
Protein expression	GST-O3-domain-F	CGTGGATCCCCGGAATTCGGCAAGGATGGGAAGGATGAT
	GST-O3-domain-R	CGATGCGGCCGCTCGAGACCGGCGGCGCCACCCAATTG
Chip-qPCR	Chip-OsBIP1-F1	GGCCTGTTGAGATTGTTGCA
	Chip-OsBIP1-R1	AAGGGTTGTTCAGATTACTGT
	Chip-OsBIP1-F2	ATTTGTGATGGCAAATCCACG
	Chip-OsBIP1-R2	CTGGTCGGGACCCGTTTACT
	Chip-OsBIP1-F3	ACGCCCAGTAAACGGGTCC
	Chip-OsBIP1-R3	TATAAGGGGAGATGACTTGA
	Chip-OsBIP1-F4	TCGCCCACGAACCCATAAA
	Chip-OsBIP1-R4	CCACCACCACCACGCGCT
	Chip-PDIL1-1-F1	CGATCGGGACCACCCGGTG
	Chip-PDIL1-1-R1	GGATACGATAAAAGCTGTGT
	Chip-PDIL1-1-F2	CTAATTTACCCGGATCCGGA

	Chip-PDIL1-1-R2	CGACTACGTACACGTACCTG
	Chip-PDIL1-1-F3	TGACGTGGCGTTGGCCGTCG
	Chip-PDIL1-1-R3	ATGCCCCTGATGAGGAGTGA
	Chip-PDIL1-1-F4	CCTCTAGTTTTAGCACATCTC
	Chip-PDIL1-1-R4	CTGAGACGACACGCTTCTCA
LUC assay	None-O3-EcoR1-F	TAGAACTAGTGGATCCATGGCGGAGCCGGACCTACT
	None-O3-BamH1-R	GCTTGATATCGAATTCTTACAAGTGAGGGCTATGGCT
	190LUC-AGPL2-F	GGCCAGTGCCAAGCTTCGTATGCCTAGGTGCACCAAC
	190LUC-AGPL2-R	AGGGTCTTGCAGATCTTTGTGCACAAGCATTCGTATCC
	190LUC-SBE1-F	GGCCAGTGCCAAGCTTACATATGCCTTTGTGCCGGGA
	190LUC-SBE1-R	AGGGTCTTGCAGATCTGGAGGAGGAAGAGGAGGTGAG
	190LUC-ISA2-F	GGCCAGTGCCAAGCTTTAGATGGCCTCTAGGGTGTG
	190LUC-ISA2-R	AGGGTCTTGCAGATCTCTTTTCGCACGGCTATTTCG
	190LUC-GBSS1-F	GGCCAGTGCCAAGCTTCCGCTGGCACCGGAGGACTA
	190LUC-GBSS1-R	AGGGTCTTGCAGATCTGTACGTCGCTCGCGTGTGCT
	190LUC-OsBiP1-F	GGCCAGTGCCAAGCTTGGGCCTGTTGAGATTGTTGCAATT
	190LUC-OsBiP1-R	AGGGTCTTGCAGATCTACGCGCATCCGCGAACCCGAT
	190LUC-PDIL1-1-F	GGCCAGTGCCAAGCTT CGGATCTGCCATCTGTGACT
	190LUC-PDIL1-1-R	AGGGTCTTGCAGATCTGAGACGACACGCTTCTCACA
	190LUC-GluA2-F	GGCCAGTGCCAAGCTTTGCTACAACCTACCAGTCCA
	190LUC-GluA2-R	AGGGTCTTGCAGATCTCCATCGCACAAGAGGAACAA
	190LUC-Glb1-F	GGCCAGTGCCAAGCTTTAGCCATTGCACATGGAGTT
	190LUC-Glb1-R	AGGGTCTTGCAGATCTCGACCTTGCTAGCCATTGAT
	190LUC-Prol14-F	GGCCAGTGCCAAGCTTCAAAGAATAGGTCAATTCCACCCA
	190LUC-Prol14-R	AGGGTCTTGCAGATCTATAGCAAGGAGAGCAAAGACGAA
Yeast one-hybrid assays	pB42AD-O3-EcoRI-F	TGCCTCTCCCGAATTCATGGAGCACGTGTTCGCCGTC
	pB42AD-O3-EcoRI-R	CGAGTCGGCCGAATTCCTACTGAAGCTCCATGTTGAC
	pLacZi-GBSS1-XhoI-F	ATCTGTCGACCTCGAGCCCTTTGTCGAGGCGTTAGT
	pLacZi-GBSS1-XhoI-R	GAGCACATGCCTCGAGACACATTTTACCCGGTCCCC
	pLacZi-AGPL2-F	GAGCACATGCCTCGAGTCTATAGAGGGGAAGGCTGCA
	pLacZi-AGPL2-R	GAGCACATGCCTCGAGAAGCTGGTGGACAGGTAGATC
	pLacZi-SBE1-F	GAGCACATGCCTCGAGACATATGCCTTTGTGCCGGGA
	pLacZi-SBE1-R	GAGCACATGCCTCGAG AGGCTCATTAGATTCGTCTCGCA
	pLacZi-ISA2-F	GAGCACATGCCTCGAGTAGATGGCCTCTAGGGTGTG
	pLacZi-ISA2-R	GAGCACATGCCTCGAG CTTTTCGCACGGCTATTTCG
EMSA	EMSA-OsBIP1-F	TGGTCCAGGTCAGACTCATGACGTCCCGGCCAACGCGACG
	EMSA-OsBIP1-R	CGTCGCGTTGGCCGGGACGTCATGAGTCTGACCTGGACCA
	EMSA-PDIL1-F	AGCCTCGTGGAGGGATGATTTGACGATGATAAGTACAGGG
	EMSA-PDIL1-R	CCCTGTACTTATCATCGTCAAATCATCCCTCCACGAGGCT
	EMSA-GBSS1-F	GCACGCTAACGTGAGTCATGTAGCGTAATTCCAAGTTCTT
	EMSA-GBSS1-R	AAGAACTTGGAATTACGCTACATGACTCACGTTAGCGTGC
	EMSA-GBSS1-F1	CTCTCTCCCGTCCCGTTGCGTCGTCATAGACAAAAGTCGG
	EMSA-GBSS1-R1	CCGACTTTTGTCTATGACGACGCAACGGGACGGGAGAGAG
	EMSA-OsGluA2-F	TTCTCCACTGACATAATGCAAAATAAGATATCATCGATGACATAG CAACTCATGCATCATATCATGCCTCTCTCAACCTA
	EMSA-OsGluA2-R	TAGGTTGAGAGAGGCATGATATGATGCATGAGTTGCTATGTCATC GATGATATCTTATTTTGCATTATGTCAGTGGAGAA
qRT-PCR	Ubiquitin-F	TGGTCAGTAATCAGCCAGTTTGG

	Ubiquitin-R	GCACCACAAATACTTGACGAACAG
	q-SSI-F	GGGCCTTCATGGATCAACC
	q-SSI-R	CCGCTTCAAGCATCCTCATC
	q-SSIIa-F	GCTTCCGGTTTGTGTGTTCA
	q-SSIIa-R	CTTAATACTCCCTCAACTCCACCAT
	q-SSIIIa-F	GCCTGCCCTGGACTACATTG
	q-SSIIIa-R	GCAAACATATGTACACGGTTCTGG
	q-SSIVa-F	GGGAGCGGCTCAAACATAAA
	q-SSIVa-R	CCGTGCACTGACTGCAAAAT
	q-GBSSI-F	AACGTGGCTGCTCCTTGAA
	q-GBSSI-R	TTGGCAATAAGCCACACACA
	q-AGPL1-F	GGAAGACGGATGATCGAGAAAG
	q-AGPL1-R	CACATGAGATGCACCAACGA
	q-AGPL2-F	AGTTCGATTCAAGACGGATAGC
	q-AGPL2-R	CGACTTCCACAGGCAGCTTATT
	q-AGPS1-F	GTGCCACTTAAAGGCACCATT
	q-AGPS1-R	CCCACATTTCAGACACGGTTT
	q-AGPS2b-F	AACAATCGAAGCGCGAGAAA
	q-AGPS2b-R	GCCTGTAGTTGGCACCCAGA
	q-SBEI-F	TGGCCATGGAAGAGTTGGC
	q-SBEI-F	CAGAAGCAACTGCTCCACC
	q-ISA2-F	ATGCCAATGCCGTTTCTCTC
	q-ISA2-R	GTGGATGTACGGATCGAGGT
	q-PUL-F	ACCTTTCTTCCATGCTGG
	q-PUL-R	CAAAGGTCTGAAAGATGGG
	q-PHOL-F	TTGGCAGGAAGGTTTCGCT
	q-PHOL-R	CGAAGCCTGAAGTGAACTTGCT
	q-GluA2-F	ACAAAGAGAAGGATGTGCTTAC
	q-GluA2-R	ATTCTTTATCCGCATTGCCAAC
	q-GluB1-F	CAAGACAAACGCTAACGCCTTC
	q-GluB1-R	TCGATAATCCTGGGTAGTATTG
	q-GluD-F	AAAGACAATTTCGGACCCTACG
	q-GluD-R	TTAGGAACTGGTAACCCCGCTG
	q-Glb1-F	AGGTTCCAGCCGATGTTCC
	q-Glb1-R	CATGCTCTCCTCGTAGCTCCTC
	q-RM1-F	TTGTGCAGCAACTACAGCTG
	q-RM1-R	CGGAGCAATGTAGTAGTTAG
	q-Prol14-F	ACAACTCCAGCAGTTTGGTG
	q-Prol14-R	CAAGGGTGGTAATGGTACTG
	q-RP10-F	CAGTTGCCAGATGATGCAGAG
	q-RP10-R	TCAACAACAACCACAGGAAGAGA
	q-RAG1-F	GTTCTCGGTATTGCTCCTCGT
	q-RAG1-R	GGCTGTAGACTTGGTGGTGGT
	q-OsBiP1-F	TGGAAAGCTGAGGAGGGAAG
	q-OsBiP1-R	CTTGACAGGTCCCATGGTCT
	q-OsBiP2-F	ATCTCCCGTACAAGGTGGTG
	q-OsBiP2-R	CTCGGCTGTCTCCTTCATCT
	q-OsBiP3-F	TACGTCTACGGCGTCAAGAA

	q-OsBiP3-R	GGAGCTTCTCCTCGTACTCC
	q-OsBiP4-F	ATGGACCACTTCGTCAAGGT
	q-OsBiP4-R	GTCGAACAGGGACTCGATCT
	q-OsBiP5-F	AGAGCATGATCCTCCTCGAC
	q-OsBiP5-R	CGTCTGCTTGTCCTTGTACG
	q-Calnexin-F	AGGAGCTTGATGAGCCTGTT
	q-Calnexin-R	CTCAAGGCCATTCTGAAGCC
	q-PDIL1-1-F	GTGCTGCTGAGGAGTTCAAG
	q-PDIL1-1-R	CCTCAGCCCAAAGTACTGGA
	q-PDIL2-3-F	GCAAGTTGGAGTTGGTGGTT
	q-PDIL2-3-R	GGGTACCGTCCAAAGGAAGA
	q-ERdj3B-F	TCATAAAGCCAGCACCAGGA
	q-ERdj3B-R	CAGACCTGCTCGGTCATTTG
	q-SDF2-F	GGTTGCGCCATGTTGATACT
	q-SDF2-R	TACCTCTTGCTGTCCACCAG
	q-Ero1-F	TGTGTCGGCTTAGGGATTGT
	q-Ero1-R	GGCTTCTTGAATGGCTCAGG
	q-Fes1C-F	AAAGAACAGGCAGAGGGTGT
	q-Fes1C-R	TGCCGATCCTCCAGTGAAAT
	q-Sar1d-F	GAGCAGGAGCTGTGCTACTA
	q-Sar1d-R	TGACATCCACCTGAAGCCAT
	q-OsbZIP50-F	GGAAGGAGAATGAGGTGGCT
	q-OsbZIP50-R	TCCCTCGATTTCATGGCAGA
	q-OsbZIP39-F	TCCAAGGGAGGCTGGTAATG
	q-OsbZIP39-R	GGAGCTCTTGAAAGGAAGCG
semi-RT	RT-Actin1-F	CCAAGGCCAATCGTGAGAAG
	RT-Actin1-R	AAGGAAGGCTGGAAGAGGAC
	OsbZIP50-S-F	GAGCAAGAAGAAGAGGAGGC
	OsbZIP50-S-F	CTTCTTTCCGGTTACCGTCG